Liquid crystalline lipid nanoparticles for combined delivery of curcumin, fish oil and BDNF: In vitro neuroprotective potential in a cellular model of tunicamycin-induced endoplasmic reticulum stress

Miora Rakotoarisoa, Borislav Angelov, Markus Drechsler, Valérie Nicolas, Thomas Bizien, Yulia E Gorshkova, Yuru Deng, Angelina Angelova

Smart Materials in Medicine 3 (2022) 274–288

Contents lists available at ScienceDirect

Smart Materials in Medicine

journal homepage: www.keaipublishing.com/en/journals/smart-materials-in-medicine/

Liquid crystalline lipid nanoparticles for combined delivery of curcumin, fish oil and BDNF: *In vitro* neuroprotective potential in a cellular model of tunicamycin-induced endoplasmic reticulum stress

Miora Rakotoarisoa [a], Borislav Angelov [b], Markus Drechsler [c], Valérie Nicolas [d], Thomas Bizien [e], Yulia E. Gorshkova [f], Yuru Deng [g], Angelina Angelova [a,*]

[a] Université Paris-Saclay, CNRS, Institut Galien Paris-Saclay, F-92290, Châtenay-Malabry, France
[b] Institute of Physics, ELI Beamlines, Academy of Sciences of the Czech Republic, Na Slovance 2, CZ-18221, Prague, Czech Republic
[c] Keylab "Electron and Optical Microscopy", Bavarian Polymerinstitute (BPI), University of Bayreuth, Universitätsstrasse 30, D-95440, Bayreuth, Germany
[d] UMS-IPSIT MIPSIT, Université Paris-Saclay, Inserm, CNRS, Ingénierie et Plateformes au Service de l'Innovation Thérapeutique (IPSIT), 92296 Châtenay-Malabry, France
[e] Synchrotron SOLEIL, l'Orme des Merisiers, Saint-Aubin - BP 48, 91192, Gif-sur-Yvette Cedex, France
[f] Frank Laboratory of Neutron Physics, Joint Institute for Nuclear Research, Joliot-Curie Str. 6, 141980, Dubna, Russia
[g] Wenzhou Institute, University of Chinese Academy of Sciences, No.1, Jinlian Road, Longwan District, Wenzhou, Zhejiang, 325001, China

ARTICLE INFO

Keywords:
Lipid liquid crystalline nanoparticles
Nanomedicine
Cubosome
Spongosome
Curcumin
Brain-derived neurotrophic factor (BDNF)
Neuroprotection
Endoplasmic reticulum stress
Tunicamycin
SAXS
Cryo-TEM

ABSTRACT

We develop multidrug-loaded cubosome and spongosome lipid nanoparticles for targeting of endoplasmic reticulum stress as a potential emerging therapeutic strategy against neuronal degeneration. The multicompartment organization of the liquid crystalline nanoparticles (LCNPs), fabricated by self-assembly, was characterized by cryogenic transmission electron microscopy (cryo-TEM) and small-angle X-ray scattering (SAXS). Monoolein-based cubosome and spongosome LCNPs co-encapsulated the natural plant-derived antioxidant curcumin, fish oil rich in ω-3 polyunsaturated fatty acids (PUFA), and the neurotrophin brain-derived neurotrophic factor (BDNF), which is of vital need for neurogenesis. The neuroprotective properties of the nanoparticles were *in vitro* investigated in a cellular model of tunicamycin-induced endoplasmic reticulum (ER) stress using differentiated human neuroblastoma SH-SY5Y cells deprieved from serum. The intracellular accumulation of aggregates of misfolded proteins, typical for the ER stress process, was analyzed by fluorescence microscopy co-localization imaging and ER staining. The performed cellular bioassays established that the BDNF-loaded LCNPs enhanced the neuronal cell survival. The diminution of the tunicamycin-induced ER stress upon internalization of neuroprotective nanoparticles was quantified *via* the changes in the Thioflavin T fluorescence, which is a sensitive marker of protein aggregation. LCNPs with multi-drug loading appear to be promising candidates to face the challenges in neuroprotective nanomedicine development by exploiting ER-stress targeting mechanisms.

1. Introduction

Current treatments of neurodegenerative diseases are of limited efficacy and indicate the need of alternative approaches, which account for the fact that neurodegenerative disorders involve multiple risk factors [1–6]. Besides of environmental factors and genetic mutations, the deficiency of neurotrophic factor proteins such as brain-derived neurotrophic factor (BDNF), the overproduced reactive oxygen species (ROS) causing oxidative stress, DNA damage, and mitochondrial dysfunction, the altered proteostasis, the deposition of senile plaques and the formation of neurofibrillary tangles from misfolded proteins and pathological protein aggregates, as well as the altered lipid metabolism causing metabolic stress, have been suggested to favor neuronal cell death and neuroinflammation [7–15]. Protein misfolding and aggregation are typical for Alzheimer's and Parkinson's diseases and have been a focus of intensive research [16,17]. Novel therapeutic strategies, aiming at slowing down the neuronal cell loss in the progression of the neurodegenerative diseases, consider the involved subcellular and molecular-level mechanisms of these disorders [18,19].

Endoplasmic reticulum (ER) stress is an impairment of the ER

* Corresponding author.
E-mail address: angelina.angelova@universite-paris-saclay.fr (A. Angelova).

https://doi.org/10.1016/j.smaim.2022.03.001
Received 31 January 2022; Received in revised form 7 March 2022; Accepted 8 March 2022
Available online 15 March 2022

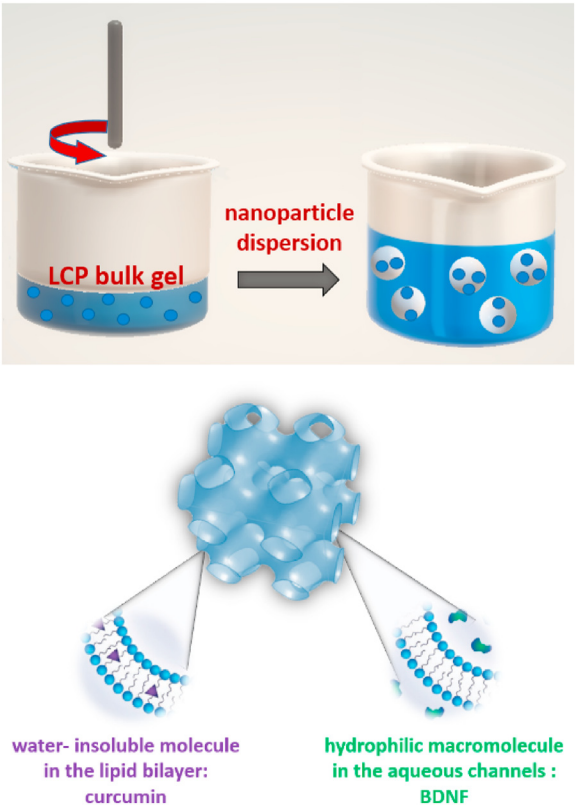

Fig. 1. Formation of liquid crystalline nanoparticles (cubosomes) by agitation-mediated dispersion of a bulk lipid cubic phase (Top panel) and a schematic presentation of the 3D supramolecular organization of a cubosome liquid crystalline nanoparticle derived from a primitive lipid cubic phase (*Im3m* crystallographic space group) (Bottom panel). The hydrophobic phytochemical curcumin (CU), chosen for drug co-encapsulation in the nanocarriers, can partition in the lipid bilayer membrane compartments of the cubosomes (bottom left), while the hydrophilic brain derived neurotrophic factor (BDNF) protein can be entrapped in the aqueous channel compartments (bottom right).

membrane functioning that is associated with the pathogenic mechanisms of a number of diseases including the neurodegenerative Alzheimer's, Parkinson's, and Huntington's diseases, amyotrophic lateral sclerosis (ALS), brain ischemia, and various peripheral neuropathies [20–27]. The endoplasmic reticulum organelle comprises a three-dimensional (3D) membrane structure, which plays a key role in protein maturation, the intracellular trafficking of secreted and membrane-associated proteins, as well as in protein modification [28–30]. It is responsible for the post-translational processing of proteins, like disulfide bond formation and N-linked glycosylation, which are determinant for the proper protein folding. ER disturbance by abnormal accumulation of unfolded or misfolded proteins, acting as toxic aggregates, can activate the ER stress-mediated apoptotic pathway in the cells [31–35]. The ER compartment is involved also in other vital processes such as the lipid biosynthesis, synthesis and transport of steroids, and the maintenance of calcium homeostasis. Therefore, ER stress is critically involved in the neuronal survival and damage as the ER stress may provoke neuronal cell death [36–38].

Nanosized drug delivery systems have opened innovative directions in nanomedicine development against neurodegenerative diseases [39–44]. By combining two or more therapeutic compounds in a single nanocarrier, they may be expected to achieve simultaneously (i) a reduction of the ROS levels responsible for the oxidative stress in the neuronal tissues, (ii) a diminishment of the damage of lipids, nucleic acids, and proteins, as well as (iii) a recovery from mitochondrial dysfunction and the abnormal changes occurring in the intracellular mitochondrial pathway [45–49]. Thus, multidrug-loaded nanocarriers may inhibit or hamper the cellular apoptosis signaling pathways. Such a neuronal regeneration strategy presents a new expectation for repairing neuronal damages.

Of particular interest are amphiphilic lipid-based nanocarriers, including liposomes and liquid crystalline nanoparticles (LCNPs) with inner self-assembled structures (cubosomes, spongosomes and hexosomes) [50–54]. They have a capacity for co-encapsulation of various active pharmaceutical ingredients, which can be either hydrophilic or lipophilic compounds attractive for drug delivery applications. Such nanocarriers can improve the bioavailability and ensure the protection of unstable encapsulated biomolecules. The lipids employed for their formulation are usually naturally occurring species and may display affinity for fusion to biological membranes. In addition to enhancing the drug bioavailability, the self-assembled lipid-based nanocarriers appear to be biodegradable and with low toxicity for *in vivo* applications [55]. In recent years, liquid crystalline nanoparticles of the cubosome type have been designed for central nervous system (CNS) targeting [43,45,56–58]. Cubosomes [59–61] can be produced by dispersion of liquid crystalline assemblies generated from lyotropic lipid cubic phases (Fig. 1, top panel). These nanoparticles include a dense core of periodically ordered bicontinuous lipid bilayer membranes that comprise a nanochannel architecture with high encapsulation potential for either hydrophilic proteins (or peptides) and poor water-soluble antioxidant agents [62–64]. Cubosome particles (Fig. 1, bottom panel) have much higher surface area per volume as compared to micellar and lamellar structures.

In the present work, we investigate a new hypothesis of whether liquid crystalline nanocarriers for combined delivery of neuroprotective molecules may provide protection and diminution of intracellular ER stress, in the perspective to halt the neuronal degeneration. For this purpose, we designed novel multidrug-loaded liquid crystalline nanoparticles starting with a lipid cubic membrane structure (Fig. 1), which is advantageous for co-encapsulation of hydrophilic and hydrophobic therapeutic substances. The choice of the bioactive molecules promoting the neuronal survival, *i.e.* (i) brain-derived neurotrophic factor (BDNF), (ii) fish oil (FO), and (iii) curcumin (CU), was done for the following reasons:

(i) Neurotrophins are needed for the growth, differentiation, and survival of neurons [65–67]. Regeneration of neuronal function can be achieved by enhancing the adult neurogenesis through endogenous administration of neurotrophic growth factors, among other neuro-regenerative mechanisms [65–69]. However, the structure of the brain, which is protected by the blood-brain barrier (BBB), limits the transport of macromolecular drugs, which causes challenges in clinical trials. The deficiency of neurotrophic factors has been defined as a risk factor of many neurodegenerative disorders [68–70]. By activating the neurotrophin receptors (*e.g.*, TrkB), these proteins support the maintenance of neuronal functions, the synaptic plasticity of developing and mature neurons, and the neuronal protection from injury and toxins [67,68]. Exogenous BDNF is required for neurogenesis as well as to compensate the decreased expression of the neurotrophic proteins in the neurodegenerative diseases [69]. Despite of its significance, the therapeutic potential of BDNF is restricted due to its short half-life (<10 min) in the circulation and the inability to cross the BBB because of its relatively large size as a dimeric protein (27 kDa) [69]. Recently developed nanoscale materials have shown promising safety and efficacy profiles for the encapsulated BDNF protein, BDNF-derived peptides or the BDNF gene, which have been delivered to the central and the peripheral nervous systems with enhanced bioavailability [71–77].

(ii) Fish oil (FO) is a rich source of bioactive ω-3 polyunsaturated fatty acid (ω-3 PUFAs) including docosahexaenoic acid (DHA; 22:6 n-3)

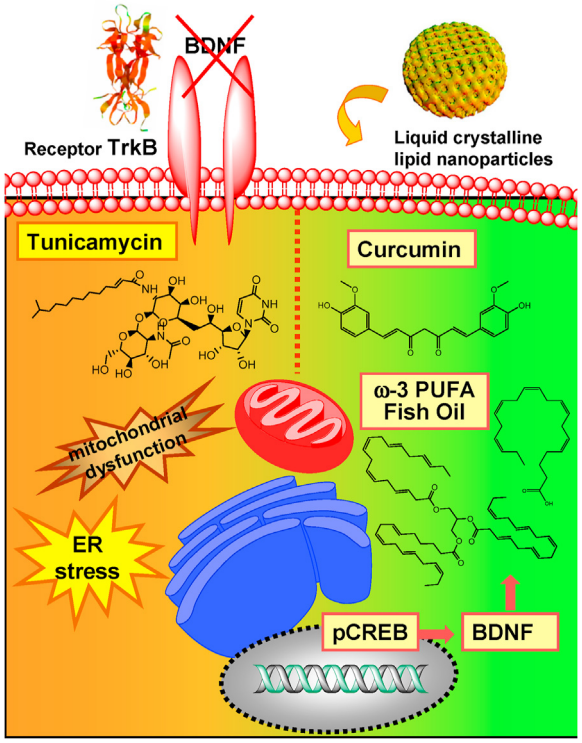

Fig. 2. Schematically presented cellular neurodegeneration model, created with differentiated human neuroblastoma SH-SY5Y cells that are subjected to tunicamycin (TUN)-induced endoplasmic reticulum (ER) stress. Serum starvation provokes oxidative-stress mitochondrial dysfunction and cellular apoptosis effects. ER stress caused by the neurotoxin TUN is accompanied by hampered neurotrophin BDNF/TrkB signaling due to low neurotrophin receptor expression and neurotrophin deficiency. The regenerative capacity of liquid crystalline lipid nanoparticles loaded by multiple active ingredients (curcumin as a phytochemical antioxidant, ω-3 PUFA-rich fish oil, and BDNF) is studied towards development of emergent combination therapies making use of natural plant-derived and marine-derived bioactive compounds.

and eicosapentaenoic acid (EPA; 20:5 n-3) with neuroprotective properties [78,79]. *In vitro* neuroprotective experiments performed with SH-SY5Y cells have established that ω-3 PUFAs, *e.g.* eicosapentaenoic acid (EPA) co-encapsulated in cubosome-type lipid carriers, exert a potentiation effect on the BDNF activity [80]. Moreover, it has been evidenced that neurotrophin-loaded or dual drug-loaded nanoparticles may help compensating the deficiency of the protein BDNF in disease models [45,71].

(iii) The plant-derived antioxidant curcumin (CU), which exerts neuroprotective and anti-inflammatory activities (among other beneficial health effects) [81–88] was chosen for co-delivery with BDNF. Curcumin has low bioavailability, due to its hydrophobic nature, and therefore needs drug delivery carriers [57]. The therapeutic advantages of curcumin have been broadly described in the literature [81–88]. For instance, curcumin reduces the oxidative damages and inhibits the formation of Amyloid β (1-42) oligomers and fibrils in the amyloid pathogenesis of the Alzheimer's disease [85]. In addition, curcumin can modulate the neurotrophin TrkB signaling and enhance the BDNF expression in neurodegenerative disease models [49].

Here non-lamellar LCNPs were fabricated by self-assembly using lipid mixtures based on the lyotropic lipid monoolein (MO). To evaluate the neuroprotective potential of the novel liquid crystalline nanoparticles co-loaded with curcumin (CU), ω-3 PUFA-rich fish oil (FO), and brain-derived neurotrophic factor (BDNF), we elaborated an *in vitro* model of ER stress with tunicamycin-treated human neuroblastoma SH-SY5Y cells, which were initially differentiated by retinoic acid and deprived of fetal bovine serum (FBS). Tunicamycin (TUN) is a nucleoside antibiotic known to induce ER stress [89–91]. TUN can act as an N-linked glycosylation inhibitor. However, N-linked glycosylation is a key early step in the folding of most proteins that takes place within the ER organelle. The inhibition of the proper folding provokes the accumulation of misfolded proteins in the ER compartment, which is a major hallmark of ER stress. Unfolded protein response (UPR), activated after the application of TUN as an ER stress-inducer, is characterized by a cessation of the global protein synthesis and can favor apoptotic pathways. The cytosolic face of the rough ER is the site of the protein synthesis where the neurotrophin receptor production is hampered in the neuronal cells. Thus, tunicamycin diminishes also the neurotrophin TrkB receptor expression because of the induced ER stress. The main features of the created here *in vitro* model of neuronal cell degeneration and nanoparticle-mediated regeneration are depicted in Fig. 2.

Table 1
Representative mixed compositions and mass proportions of monoolein (MO) lipid, amphiphilic PEGylated agent TPGS-PEG$_{1000}$, ω-3 PUFA-rich fish oil (FO), and curcumin (CU) for preparation of liquid crystalline nanoparticles by thin lipid film hydration and self-assembly.

weight ratio (wt/wt)	MO (g)	TPGS-PEG$_{1000}$ (g)	FO (g)	CU (g)
0/100 FO:MO	0.1	0.027	–	–
32/68 FO:MO	0.1	0.027	0.0544	–
32/68 FO:MO	0.1	0.027	0.0544	0.0074
0/100 FO:MO	0.1	0.027	–	0.0074

2. Material and methods

2.1. Materials and sample preparation

Monoolein (MO) with purity >99% was obtained from Hampton Research. The PEGylated amphiphile, D-α-tocopheryl poly(ethylene glycol)1000 succinate (denoted as TPGS-PEG$_{1000}$) was purchased from Sigma Aldrich. Fish oil (FO) (from menhaden, crude source of ω-3 polyunsaturated fatty acids), *cis*-4,7,10,13,16,19-docosahexaenoic acid (DHA) (purity ≥98%), curcumin (CU) (purity >66%), butylated hydroxytoluene (BHT), Thioflavin T (4-(3,6-dimethyl-1,3-benzothiazol-3-ium-2-yl)-N,N-dimethylaniline chloride) (Ex. 458 nm, Em. 480–520 nm), and retinoic acid (RA) were purchased from Sigma Aldrich as well. The water was of MilliQ quality (Millipore Corp., Molsheim, France) and was used for preparation of a phosphate buffer solution (NaH_2PO_4/Na_2HPO_4, 1×10^{-2} M, pH 7, p.a. grade, Merck). Human BDNF for structural experiments was obtained from R&D Systems (BioTechne Ltd, UK) as well as from Sigma Aldrich for the cell culture studies. For the cell culture experiments, Dulbecco's modified Eagle's Medium (DMEM), streptomycin-penicillin, phosphate buffered saline (PBS), trypsin, ethylenediaminetetraacetic acid EDTA, and 3-(4,5-Dimethylthiazol-2-yl)-2,5-diphenyl tetrazolium bromide (MTT) were supplied by Sigma-Aldrich. Fetal bovine serum (FBS) was provided by Thermo Fischer Scientific (Illkirch, France). Fluorescent staining dyes and kits were purchased from Thermo Fisher Scientific, Invitrogen, and Biotium.

Lipid nanoparticles were prepared by the method of hydration of a lyophilized thin lipid film followed by physical agitation in excess aqueous phase [47,48,59,92–94]. The lipid monoolein (MO), the amphiphilic stabilizer TPGS-PEG$_{1000}$, ω-3 PUFA-rich fish oil (FO), and curcumin (CU) were weighed, dissolved in chloroform and mixed at desired proportions. Typical amphiphilic compositions used for nanoparticle preparation are given in Table 1. The solvent was evaporated under a stream of a nitrogen gas for 1 h at room temperature to create a thin lipid film. The samples were lyophilized overnight under cooling to remove the excess solvent. This step was followed by the hydration of the thin film samples by an aqueous phase (1×10^{-2} M phosphate buffer), which contained butylated hydroxytoluene (BHT). The antioxidant BHT

helped ensuring the oxidative stability of the formulations. For dispersion to nanoparticles, the multicomponent assemblies were agitated by sonication and vigorous vortexing in cycles during 15 min. The lipid concentration was 10 wt% with regard to the aqueous phase. For preparation of BDNF-loaded liquid crystalline nanoparticles, the neurotrophic protein was incorporated by incubation and mixing of 1 μL BDNF stock solution (500 μg/ml BDNF) and a volume of 4 μL of lipid nanoparticles (stock concentration of 56 mM lipid monoolein in the samples). The BDNF-loaded nanoparticles were stored at 4 °C.

2.2. Synchrotron small-angle X-ray scattering (SAXS)

The methodology of the performed SAXS study at the SWING beamline of synchrotron SOLEIL (Saint Aubin, France) was analogous to the previously described [47]. The dispersed nanoparticle samples were sealed in X-ray capillaries and placed in a designed holder with (X,Y,Z) positioning. Temperature was 22 °C. The sample-to-detector distance was 3 m and the X-ray beam spot size on the samples was 25 × 375 μm^2. The patterns were recorded with a two-dimensional Eiger X 4 M detector (Dectris, Baden-Daettwil Switzerland) at 12 keV allowing measurements in the q-range from 0.00426 to 0.37 Å^{-1}. The q-vector was defined as $q = (4\pi/\lambda) \sin\theta$, where 2θ is the scattering angle. The synchrotron radiation wavelength was $\lambda = 1.033$ Å and the exposure time was 500 ms. The q-range calibration was done using a standard sample of silver behenate (d = 58.38 Å). An average of five spectra per sample was acquired. Data processing of the recorded 2D images was performed by the FOXTROT software as previously indicated [47].

2.3. Cryogenic transmission electron microscopy (cryo-TEM)

The methodology of the cryo-TEM study was similar to that in the previous work [48]. In brief, a sample droplet of 2 μL was put on a lacey carbon film covered copper grid (Science Services, Munich, Germany), which was hydrophilized by glow discharge (Solarus, Gatan, Munich, Germany) for 30s. Most of the liquid was then removed with blotting paper, leaving a thin film stretched over the lace holes. The specimen was instantly shock frozen by rapid immersion into liquid ethane and cooled to approximately 90 K by liquid nitrogen in a temperature and humidity controlled freezing unit (Leica EMGP, Wetzlar, Germany). The temperature and humidity were monitored and kept constant in the chamber during all sample preparation steps. The specimen was inserted into a cryo-transfer holder (CT3500, Gatan, Munich, Germany) and transferred to a Zeiss EM922 Omega energy-filtered TEM (EFTEM) instrument (Carl Zeiss Microscopy, Jena, Germany). Examinations were carried out at temperatures around 90 K. The TEM instrument was operated at an acceleration voltage of 200 kV. Zero-loss-filtered images (DE = 0 eV) were taken under reduced dose conditions (100–1000 e/nm^2). The images were recorded digitally by a bottom-mounted charge-coupled device (CCD) camera system (Ultra Scan 1000, Gatan, Munich, Germany) and combined and processed with a digital imaging processing system (Digital Micrograph GMS 1.9, Gatan, Munich, Germany). The sizes of the investigated nanoparticles were in the range or below the film thickness and no deformations were observed. The images were taken very close to focus or slightly under the focus (some nanometers) due to the contrast enhancing capabilities of the in-column filter of the employed Zeiss EM922 Omega. In EFTEMs, the deep underfocused images can be totally avoided.

2.4. Cellular viability determined by MTT assays

The cellular viability was determined by the tetrazolium salt test (3-(4,5-dimethylthiazol-2-yl)-2,5-diphenyl tetrazolium bromide, MTT) after SH-SY5Y cell treatment by (i) retinoic acid (RA) deprived of fetal bovine serum (FBS), (ii) tunicamycin (TUN), and (iii) studied nanoparticles. In this assay, the MTT reagent is reduced to formazan by the mitochondrial succinate dehydrogenase enzyme in the living cells. The MTT compound forms a purple precipitate, the quantity of which is proportional to the metabolic activity of the living cells. The cells were seeded at a density of 20 × 10^4 cells/well in 96-well plates. After 5 days of treatment with 10 μM retinoic acid, the RA-differentiated cells were stressed during 24 h by deprivation of FBS (*i.e.* starvation) or by incubation with an ER stress inducer (1 μM TUN). Blank (non-loaded) or BDNF-loaded nanoparticles were incubated with the cells at 37 °C for 24 h at lipid concentrations of 2.5 μM and 5 ng/ml BDNF. Untreated cells maintained in the DMEM medium were used as controls. The solution of MTT was prepared in PBS and was filtered prior use. The reagent MTT was added to the wells at a concentration of 5 mg/mL at 37 °C. After 1 h of incubation of the cells with MTT, the medium was removed, and the cells were dissolved in 100% DMSO in order to solubilize the formazan precipitate. The optical density of the samples was measured at a wavelength 570 nm using a multiwell-scanning plate reader (LT-5000 MS, Labtech). The quantification was done by averaging the measurements of a minimum six wells.

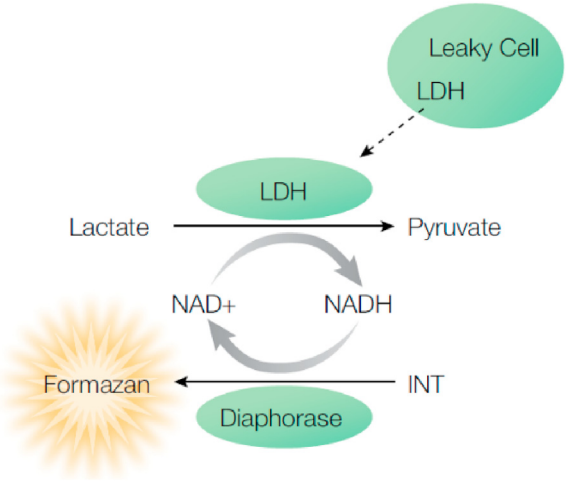

Fig. 3. In the LDH assay, the release of lactate dehydrogenase (LDH) from the damaged cells is measured by supplying lactate, NAD+ and iodonitrotetrazolium violet (INT) as enzyme substrates in the presence of diaphorase (coupled enzyme diaphorase-LDH assay). The generated red formazan product is proportional to the quantity of LDH released from the cells, and therefore to the number of lysed cells.

2.5. Cellular cytotoxicity determined by a LDH (lactate dehydrogenase) assay

The CytoTox 96® Non-Radioactive Cytotoxicity Assay kit was used to evaluate the cell death and the number of live cells following the SH-SY5Y cell treatment by (i) retinoic acid (RA) deprived of fetal bovine serum (FBS), (ii) tunicamycin (TUN), and (iii) nanoparticles. This assay quantitatively measures the amount of lactate dehydrogenase (LDH), a stable cytosolic enzyme that is released upon cell lysis. The released protein LDH in the culture supernatants is measured within 30-min by a coupled enzyme assay (Fig. 3), which results in the conversion of a tetrazolium salt (iodonitrotetrazolium violet, INT) into a red formazan product. The generated red color intensity is proportional to the number of lysed cells. The absorbance data are collected using a standard 96-well plate reader at a visible wavelength (490 nm).

To measure cell death, following cell starvation and incubation with BDNF (5 ng/ml)-loaded LCNPs (48 h), the SH-5Y5Y cells were seeded at a density of 20 × 10^4 cells/well in 96-well plates. 50 μL aliquots from all test and control wells were transferred to a fresh 96-well flat-clear-bottom plate and 50 μL of the CytoTox 96® reagent was added. The plate was protected from light during 30 min incubation at room temperature. Then, 50 μL of stop solution was added before recording the absorbance at a wavelength 490 nm (or 492 nm) within 1 h. The quantification of cytotoxicity (cellular death) was done using the relationship.

$$\text{Percent cytotoxicity} = \frac{\text{Experimental LDH Release } (OD_{490})}{\text{Maximum LDH Release } (OD_{490})} X \ 100$$

The CytoTox 96® Assay indirectly measures the lactate dehydrogenase activity of the enzyme, which is present in the cytoplasm of intact cells. Therefore, cell number quantitation can only be done if the cells are lysed to release the LDH enzyme from the cells. To measure the number of live cells following the different treatments, the medium in the plate containing the seeded cells was removed after taking aliquots for the cytotoxicity assay. The cellular samples of interest were lysed by adding 15 µl of Lysis 10X Solution [9% (v/v) TritonR X-100 in water] per 100 µl of culture medium, followed by incubation at 37 °C for 45–60 min. CytoTox 96® Reagent (50 µl) was added to each supernatant sample, and the enzymatic reaction was allowed to proceed for 30 min at room temperature under protection from light. The enzymatic assay was then stopped by adding 50µl/well of stop solution. The absorbance was recorded at a wavelength 490 nm using a plate reader.

2.6. Fluorescence microscopy imaging of living cells

The cells were seeded at a density of 40 × 10^4 cells/well in 6-well plates and treated with tunicamycin and BDNF-loaded LCNPs. Fluorescent microscopy images of living cells were acquired with a ZEISS AXIO Observer Z1 video microscope equipped with a 63 × objective and a CoolSnap HQ2 camera. CALIBRI/LED (Light Emitting Diodes) of four wavelenghts (365 nm, 470 nm, 555 nm, and 590 nm) were available as excitation sources. The images were visualized using the ZEISS ZEN microscope software (Version 3.1, Germany). The excitation and emission wavelength settings were the following: Thioflavin T (ThT) (Ex. 470 nm, EM BP 530/50 nm), ER-Tracker™ Blue White DPX dye (Ex. LED 365 nm, EM BP 445/500 nm) and MitoView™ Green (Ex. 470 nm, EM BP 530/50 nm). Each fluorescent channel was recorded sequentially, as opposed to simultaneously, in order to avoid channel overlap. For fluorescence quantification, the images were converted into 8-bit and treated through the mean grey value analysis of the *ImageJ* software. A polygon (region of interest, ROI) with the same area was selected for each image in order to normalize and compare the fluorescence intensity data per cell.

2.7. Human free BDNF quantification by Quantikine® ELISA immunoassay

The concentrations of human free brain-derived neurotrophic factor (BDNF) in cell culture supernates were determined using Quantikine® ELISA Human Free BDNF Immunoassay kit (Bio-Techne Ltd./R&D Systems, UK) following the manufacturer's instructions. Briefly, the 96 well plates were pre-coated with a monoclonal antibody specific for human free BDNF. BDNF standards and samples were pipetted and incubated into the wells for 2 h and any free BDNF present was bound by the immobilized antibody. An enzyme-linked monoclonal antibody, specific for human free BDNF, was added to the wells for 1 h. All of the incubation stages were conducted at room temperature. Then, a procedure of a total of 3 washes with washing buffers was performed to remove any unbound antibody-enzyme reagent. A substrate solution was added to the wells for 30 min. The color was developed in the wells proportionally to the amount of free BDNF bound in the initial step. The color development was stopped with a stop solution and the color intensity was measured by a plate reader. The absorbance at 450 nm was measured within 30 min after stopping the reaction.

The total protein concentration was measured by the Bradford Protein Assay (BSA). The stock solution of BSA was with a concentration 2 mg/mL in PBS, from which a calibration range of seven concentrations was prepared. 20 µL of BSA standard solutions or cell lysate samples were mixed in the wells with 180 µl Bradford reagent. The optical density of every well was measured by a microplate reader set to a wavelength 595 nm. The total protein content was used for normalization of the determined BDNF protein amount in the studied samples.

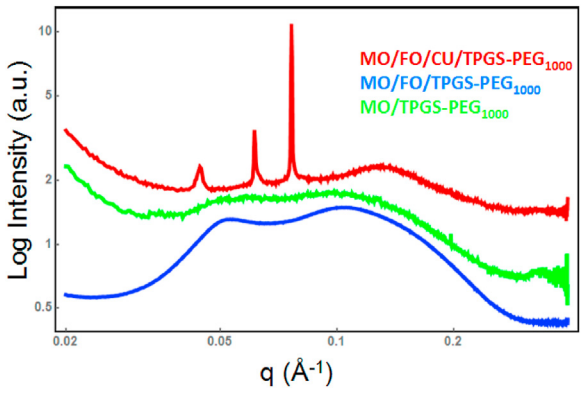

Fig. 4. Synchrotron small-angle X-ray scattering (SAXS) patterns of multicomponent liquid crystalline lipid nanoparticles with encapsulated neuroprotective molecules [MO/FO/CU/TPGS-PEG_{1000}]. The dispersed nanoassemblies are stabilized by the PEGylated amphiphilic agent D-α-tocopheryl-poly(ethylene glycol)1000 (TPGS-PEG_{1000}). The nanoparticle dispersions are fabricated with 5 wt % lipid content and 95 wt % aqueous medium. Aqueous phase composition: 1 × 10^{-2} M phosphate buffer containing butylated hydroxytoluene (BHT). Temperature: 22 °C.

2.8. Statistical analysis

The data were expressed as mean ± standard deviation (SD) of three independent experiments. The results were analyzed by the Tukey test after one-way analysis of variance. The probability values $p < 0.05$ were considered statistically significant across the treatment groups.

3. Results and discussion

3.1. Structural characterization of the designed liquid crystalline lipid nanoparticles

3.1.1. SAXS investigation of dispersed cubosome and spongosome lipid nanoparticles

Fig. 4 shows the SAXS patterns of dispersed MO/TPGS-PEG_{1000} lipid nanoparticles as well as of MO/FO/TPGS-PEG_{1000} and MO/FO/CU/TPGS-PEG_{1000} nanocarriers, which are loaded with neuroprotective bioactive ingredients, *i.e.* ω-PUFA rich fish oil (FO) and curcumin (CU). The PEGylated amphiphile TPGS-PEG_{1000}, included in the studied multicomponent assemblies, provided steric stabilization of the nanoparticle dispersions. The structural effect of fish oil on the inner organization of the PEGylated liquid crystalline nanoparticles (Fig. 4, blue plot) is presented together with that of encapsulated curcumin (Fig. 4, red plot). The blank MO/TPGS-PEG_{1000} and the fish oil-loaded MO/FO/TPGS-PEG_{1000} nanoparticles displayed scattering curves typical for dispersed lipid membranes as precursors of bicontinuous cubic phases. Two correlation peaks $q_1 = 0.05$ Å^{-1} and $q_2 = 0.11$ Å^{-1} were observed for the LCNPs in the lack of encapsulated curcumin. The first correlation peak corresponds to a precursor of a cubic *Im3m* primitive cubic phase structure, which is dispersed into nano-objects [94]. The position of the second correlation peak is close to the one of dispersed sponge-type lipid membranes [43,92]. These structural data suggest that the studied amphiphilic compositions may yield nanoparticles with domain organization, cubosomal intermediates, or coexistences of cubosomes and spongosomes in the formulations [43,92–94].

The recorded Bragg reflections in the SAXS pattern of the curcumin and fish oil dual-loaded MO/FO/CU/TPGS-PEG_{1000} LCNPs identified the formation of cubosome nanoparticles with an inner cubic lattice structure of the primitive cubic (*Im3m*) space group (Fig. 4, red plot). The *q*-vector positions of the Bragg peaks centered at $q = 0.044$ Å^{-1}, 0.062 Å^{-1} and 0.076 Å^{-1} determined a unit cubic cell lattice parameter $a_{Q(Im3m)} =$ 20.19 nm for the dispersed cubosome particles. The broad correlation

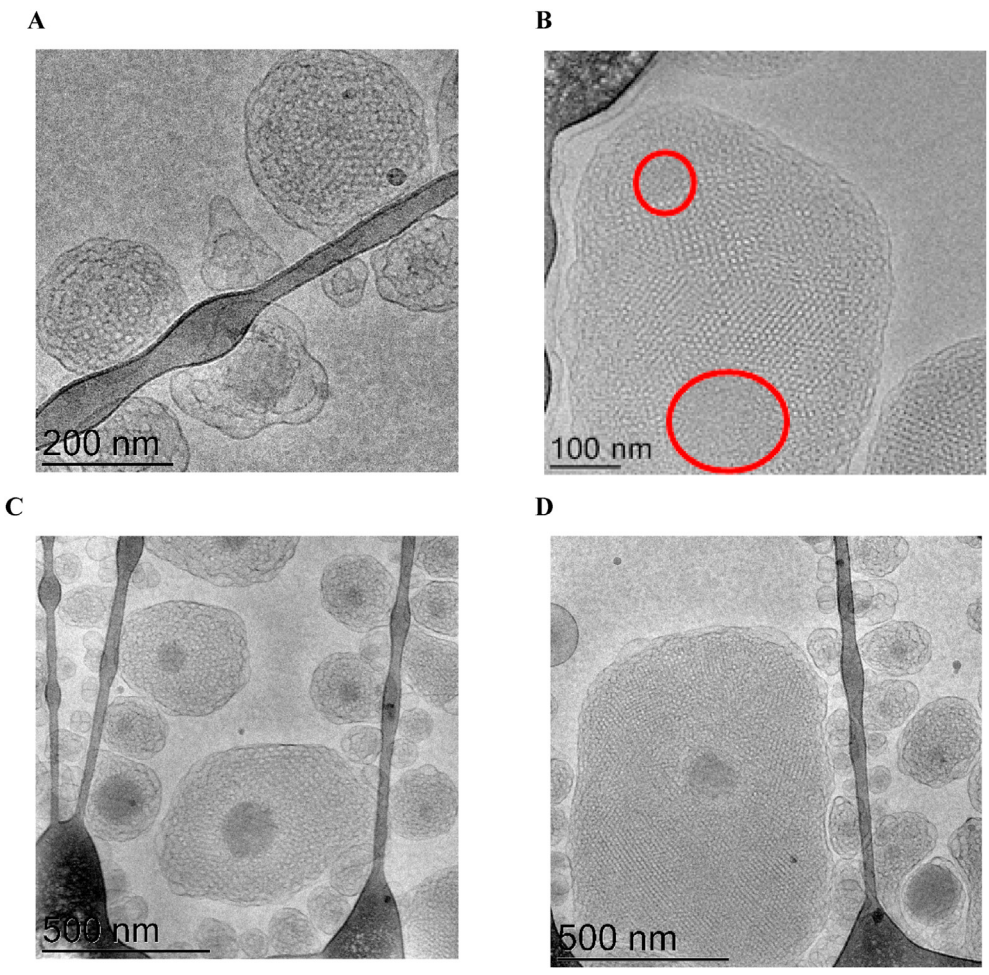

Fig. 5. Cryo-TEM images of dispersed liquid crystalline lipid nanoparticles with encapsulated fish oil (rich in ω-3 PUFA) and phytochemical antioxidant. The multicomponent assemblies [MO/FO/CU/TPGS-PEG_{1000}] are stabilized by a PEGylated amphiphilic stabilizer D-α-tocopheryl-poly(ethylene glycol) 1000 (TPGS-PEG_{1000}). The incorporated guest molecules cause distortions of the long-range order of the bicontinuous lipid membranes and lead to formation of cubosomal intermediates and sponge type nanoparticles (panel (**A**)); cubosomes with inner oil-rich domains (outlined by red color in panel (**B**)); or inner areas rich in curcumin (darker domains in the core of the liquid crystalline lipid nanoparticles) in panels (**C**) and (**D**).

peak centered at $q = 0.135$ $Å^{-1}$ indicated that the cubosomes coexist with a portion of nanoparticles involving bicontinuous sponge membranes with no periodic organization.

The small shift, observed in the position of the correlation peak centered at $q = 0.135$ $Å^{-1}$ for the MO/FO/CU/TPGS-PEG_{1000} LCNPs (Fig. 4, red line) with regards to its position at approximately $q = 0.11$ $Å^{-1}$ in the SAXS patterns of the other two types of LCNPs can be explained by the density of the lipid membranes and their hydration level in the dispersed lipid assemblies. We have previously shown that the early stages of lipid membrane ordering during the bilayer vesicle-to-cubosome particle transition are characterized by broad peaks in the scattering patterns due to the small number of correlated lipid membranes [93]. The intermediate transition states correspond to higher hydration levels of the inner lipid nanoparticle organization, which is of the swollen type and displays scattering peaks at smaller q-vector values. The topological transition associated with membrane reorganization into a bicontinuous three-dimensional membrane leads to progressive squeezing of the water and formation of porous structures of varying densities [92]. A higher density of the lipid bilayers corresponds to LCNPs of less hydrated internal structure. In the present case, LCNPs compositions involving curcumin appear to generate more densely packed nanoscale structures as compared to those involving fish oil only (Fig. 4). Thus, the shift from $q = 0.11$ $Å^{-1}$ to $q = 0.135$ $Å^{-1}$ may indicate that curcumin slightly reduces the hydration of the dispersed lipid membranes.

LCNPs nanostructures containing brain-derived neurotrophic factor (BDNF) were obtained by incubation with the neurotrophin stock solution as described in Methods. The protein BDNF (as a high-affinity ligand of the neurotrophin receptor TrkB) exerts its neuroprotective activity at very low concentrations (≤nanogram/mL range). At the studied low protein concentration, the SAXS patterns of the BDNF-associated (MO/FO/CU/BDNF) nanoparticles did not differ from the LCNPs encapsulating fish oil and curcumin (MO/FO/CU) (see the red plot for the MO/FO/CU/TPGS-PEG_{1000} nanoassemblies in Fig. 4).

3.1.2. Morphological characterization of dispersed liquid crystalline lipid nanoparticles by Cryo-TEM imaging

The dispersed liquid crystalline lipid nanoparticles were examined by Cryo-TEM. The images presented in Fig. 5 show the topologies of the cubosome and spongosome lipid nanoparticles loaded with bioactive ingredients. A closer inspection of the Cryo-TEM micrographs revealed the domain inner organization of the LCNPs and a phase separation resulting from the encapsulation of ω-3 PUFA-rich fish oil and curcumin in the host lipid particles. Depending on the composition, MO/FO/TPGS-PEG_{1000} or MO/FO/CU/TPGS-PEG_{1000}, the internal LCNP organization involved inner oil-rich domains (Fig. 5B) or core-shell structures with domains rich in curcumin in the core of the lipid nanoparticles (Fig. 5C and D). The established multicompartment organization of the LCNPs with internal domains, rich in fish oil and curcumin, suggests multistep mechanism of release from the dual-loaded cubosome or spongosome type lipid nanoparticles, which requires a separate investigation.

The investigated LCNP formulations were stable over at least three months. The amphiphilic TPGS-PEG_{1000} agent favors the LCNPs dispersion by impeding the aggregation. The nanoparticle sizes as a function of the content of encapsulated fish oil were studied by quasi-elastic light scattering (QELS) in our recent work [94]. The determined size distributions established a coexistence of small particles comprising dispersed vesicular membranes and precursors of cubosomes (with hydrodynamic

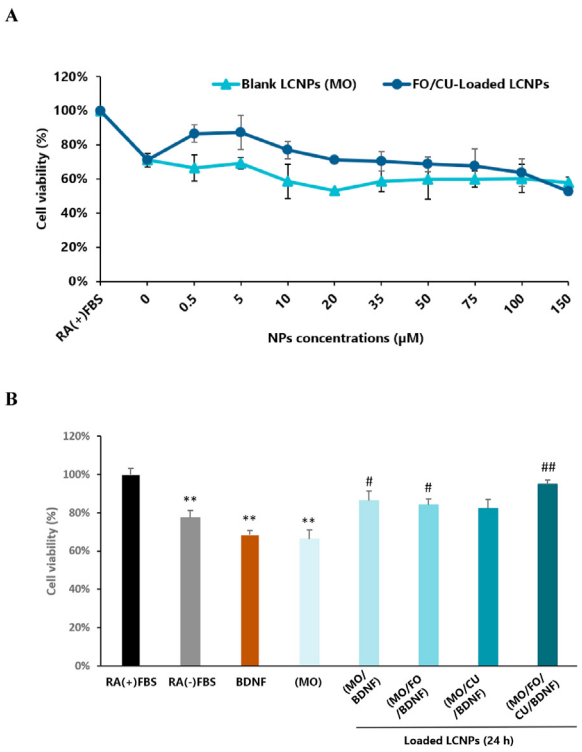

Fig. 6. Cellular viability determined by a MTT assay for **(A)** retinoic acid (RA)-differentiated SH-SY5Y cells after 24 h exposure to blank or FO/CU-loaded liquid crystalline nanoparticles at varying concentrations; and **(B)** controls *versus* treatment by LCNPs of different compositions at same lipid concentration of 2.5 μM. Significant differences were observed with **p < 0.01 *vs.* RA (+) FBS; #p < 0.05 and ##p < 0.01 *vs.* BDNF alone.

diameters of about 100 nm) and bigger particles, which correspond to LCNPs with inner self-assembled structure (cubosomes or spongosomes). Their population is characterized by a mean hydrodynamic diameter in the range 250 nm–450 nm. It has been previously emphasized that the vesicular membranes, produced upon the dispersion and sonication of the bulk liquid crystalline phase, serve as a reservoir of lipid membrane building blocks for the generation of cubosome and spongosome LCNPs [43,48,93].

3.2. Cytotoxicity of blank and multidrug-loaded liquid crystalline nanoparticles

The human neuroblastoma SH-SY5Y cells were seeded and treated with RA (10 μM) during 5 days to obtain the typical neuronal cell phenotype. Then, the cells were starved by incubation with serum (FBS)-free DMEM medium for 24 h (the condition before the cell treatment with the nanoparticles). The differentiated cells were exposed to formulations of liquid crystalline nanoparticles for 24 or 48 h. The LCNPs were loaded or not by BDNF (5 ng/ml). As viability controls, we used SH-SY5Y cells, which were not exposed to nanoparticles, *i.e.* (RA(−)FBS).

3.2.1. MTT assay with liquid crystalline nanoparticles with and without BDNF loading

The obtained MTT data (Fig. 6A and B) demonstrate that the cellular viability decreased from 100 ± 3.2% to 71 ± 4.0% for starved differentiated SH-SY5Y cells (RA(−)FBS) as compared to the RA-differentiated SH-SY5Y control cells (RA(+)FBS). The serum FBS deprivation influenced significantly (**$p < 0.01$) the cellular viability. This result established a crucial stress condition induced by the starvation.

Differentiated SH-SY5Y cells were exposed to blank or dual-loaded liquid crystalline (MO/FO/CU) nanoparticles at different

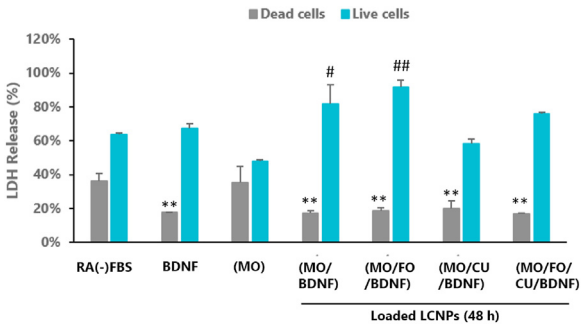

Fig. 7. Results of a LDH assay for determination of cytotoxicity of blank or loaded liquid crystalline nanoparticles in retinoic acid (RA)-differentiated SH-SY5Y cells after 48 h exposure to LCNPs formulations. Significant differences are observed for **p < 0.01 *versus* dead RA(−)FBS cells control; #p < 0.05 and ##p < 0.01 *versus* live RA(−)FBS cells control.

concentrations for 24 h (Fig. 6A). At all concentrations, the blank LCNPs presented around 60% cellular viability (*versus* control), which did not essentially differ from the cellular viability of the starved differentiated SH-SY5Y cells (RA(−)FBS at 0 μM NPs content). The FO/CU-loaded nanoparticles enhanced the cellular viability, with values from 77 to 87 ± 5.0% at concentrations between 0.5 μM and 10 μM. Above 10 μM LCNPs concentration, the viability was comparable with that of the starved cells. These results indicated that the studied nanoparticles were safe. Indeed, the FO/CU-loaded LCNPs increased the cellular viability at low concentrations and protected them from starvation-induced stress and cellular death. These results can be explained by the protective fish oil effect and the survival effects favored by the antioxidant curcumin [100–104]. A recent study has demonstrated the improvement of the stability and efficacy of fish oil nanoemulsions by co-encapsulation of FO with CU or other antioxidants [101].

The MTT results for cells exposed during 24 h to multidrug-loaded liquid crystalline (MO/FO/CU/BDNF) nanoparticles at a lipid concentration of 2.5 μM and at BDNF concentration of 5 ng/ml are shown in Fig. 6B. The MTT data established a cell viability increase from 82 ± 4.7% to 95 ± 2.1% with the single- or multidrug-loaded nanoparticles involving BDNF treatment. The obtained values did not suggest a significant cell viability difference as compared to the control RA(+)FBS cells. A more significant cell viability decrease (66 ± 4.7%, **$p < 0.01$) was observed with the blank nanoparticles (MO) with no encapsulated neuroprotective additives. These results evidenced the safety of the single- and multidrug-loaded nanoparticles as well as the significant effect of the BDNF-loaded LCNPs on the cellular survival after starvation of the RA-differentiated SH-SY5Y cells.

Interestingly, the percentage of cell survival significantly increased (#p < 0.05 and ##p < 0.01) upon treatment with BDNF-loaded LCNPs as compared to free BDNF treatment alone (Fig. 6B). This result demonstrates the advantage of using LCNPs for neuronal protection through enhancement of the effect of the neurotrophic protein. The potentiation effect of multicompartment lipid carriers, containing ω-3 PUFAs, on the BDNF activity in *in vitro* neuroprotective experiments with SH-SY5Y cells has been previously suggested [43,80]. The fact that the viability is significantly higher with the multidrug [FO/CU/BDNF]-loaded LCNPs may be due to a synergistic effect of co-encapsulated drugs in the lipid-based nanocarriers (Fig. 6B). Curcumin may mediate the intracellular BDNF signaling cascades, which are involved in the neuroprotective pathways [105–110]. Zhang et al. have reported that chronic curcumin treatments activate ERK or N-methyl-D-aspartate-CREB signaling, accelerate the expression of BDNF, and improve biochemical and behavioral changes in an AD rat model induced by ventricular inoculation of $A\beta_{1\text{-}42}$ [109]. Another study has hypothesized that the neuroprotection by curcumin can be mediated via the BDNF/TrkB-MAPK/PI-3K-CREB signaling pathway [108].

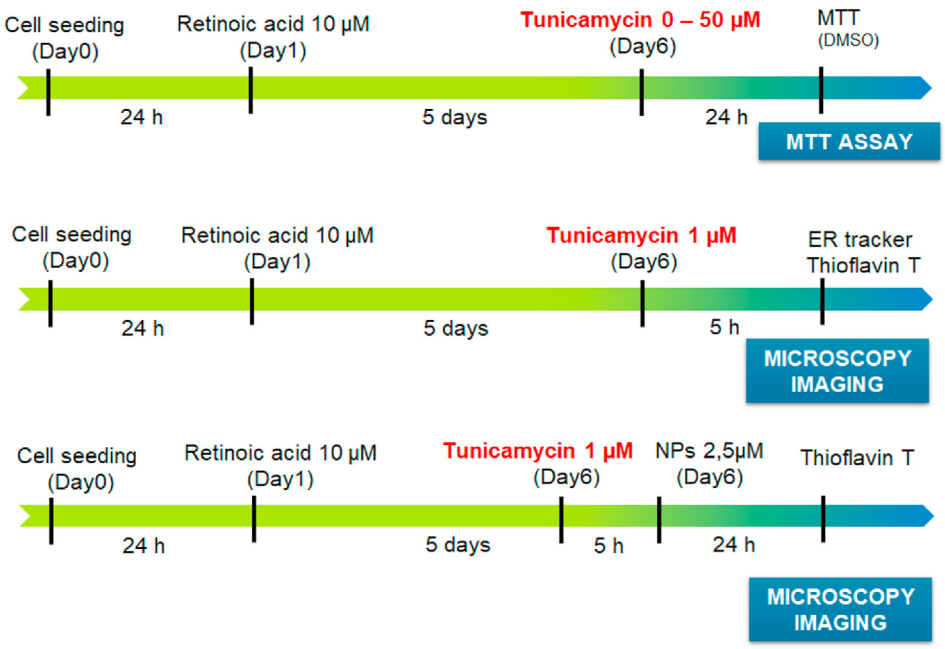

Fig. 8. Schematic presentation of the treatment protocols of differentiated human neuroblastoma SH-SY5Y cells employed for evaluation of the effect of LCNPs on the tunicamycin-induced endoplasmic reticulum stress (*in vitro* model). The fluorescent dye Thioflavin T (ThT) (5 µM) was used for cell culture staining in order to evidence the tunicamycin-induced ER stress. The ThT molecule directly interacts with the misfolded proteins in the ER organelle. It is a marker for detecting protein aggregates as a measure of the ER stress levels in the cells [98].

3.2.2. LDH assay with BDNF-loaded liquid crystalline nanoparticles

The lactate dehydrogenase (LDH) assay was used to quantify dead cells by the released LDH protein in culture supernatants upon the cell lysis due to serum starvation and treatment by BDNF(5 ng/ml)-loaded

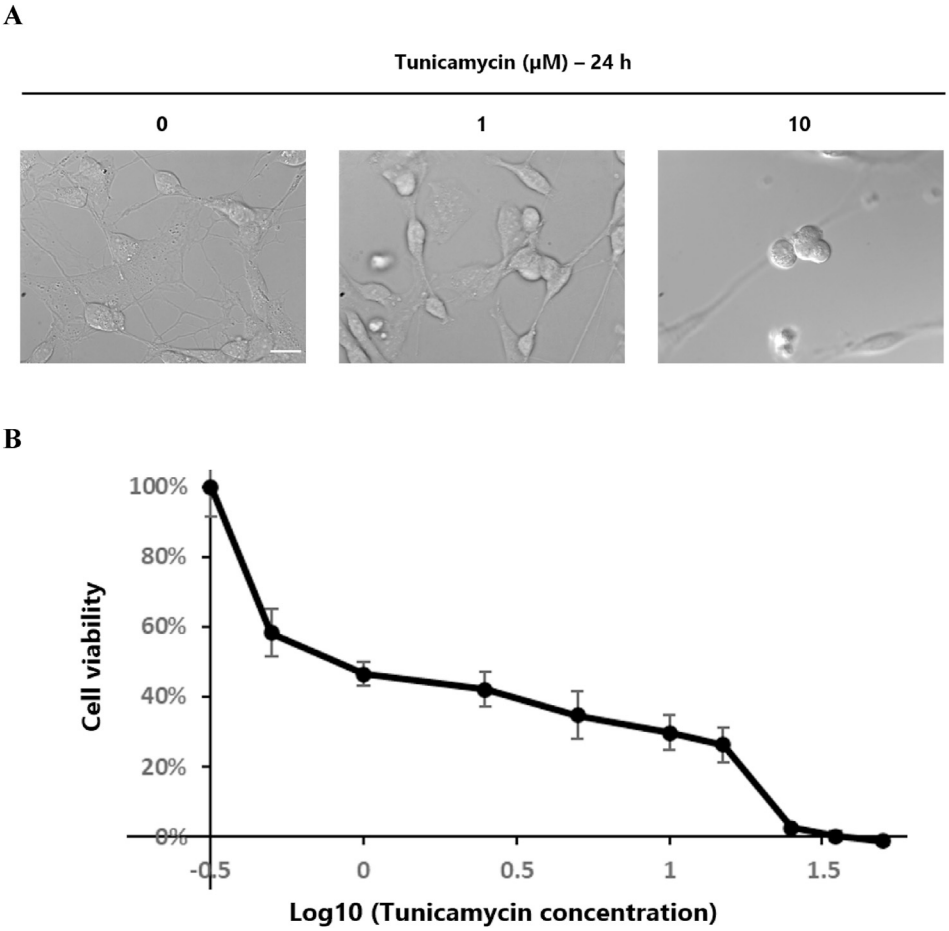

Fig. 9. Tunicamycin dose-dependent effect on cellular viability of RA-differentiated SH-SY5Y deprived of FBS. The cells were treated with different concentration of TUN for 24 h. **A)** Optical micrographs acquired by a ZEISS microscope with an objective × 63 (Scale bar: 15 µm). **B)** Cellular viability determined by a MTT assay following exposure to 0–50 µM tunicamycin (see the treatment protocol depicted in Fig. 8, middle row scheme).

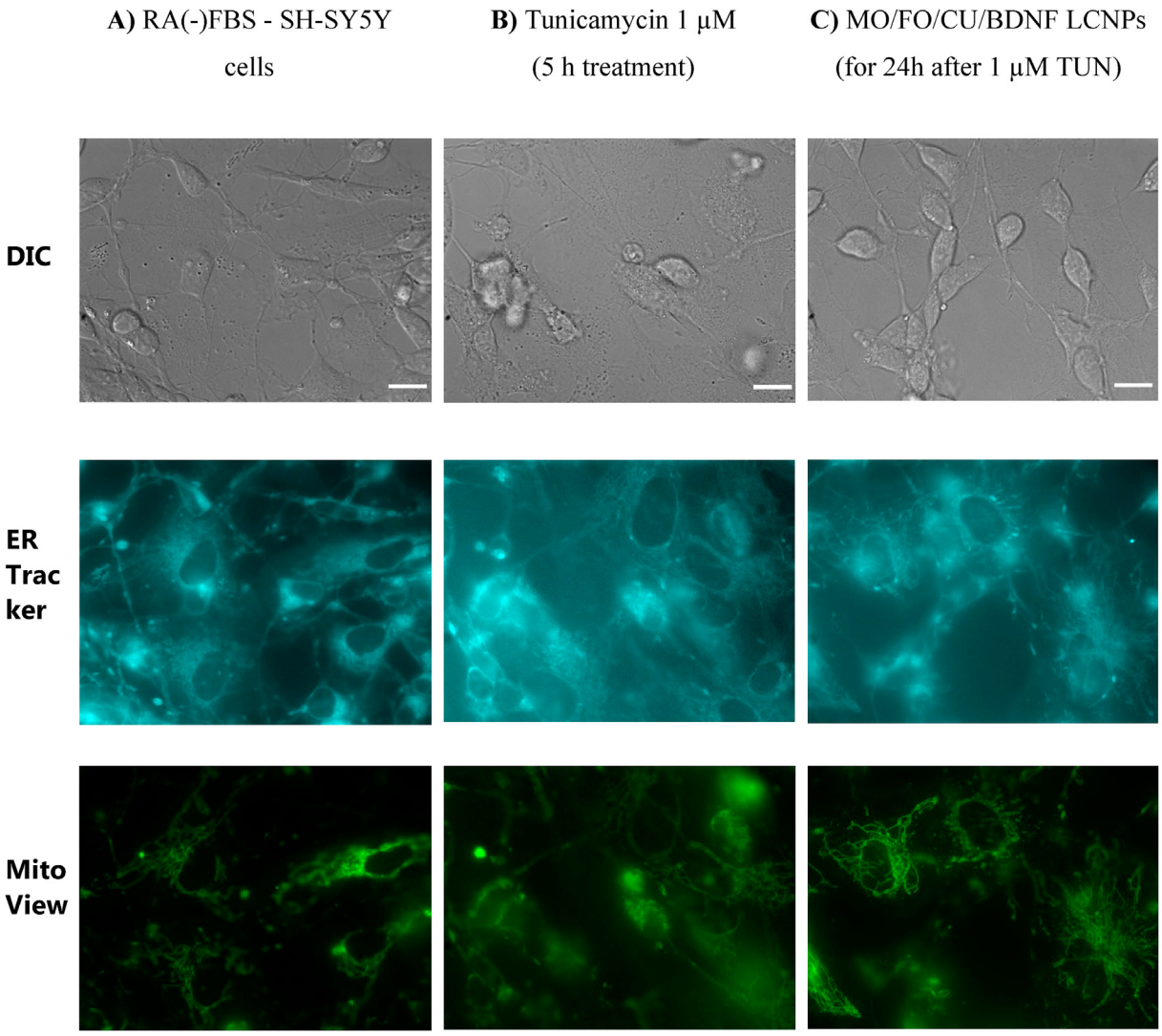

Fig. 10. Fluorescence microscopy images showing the SH-SY5Y cellular morphology (DIC images in the upper row), the endoplasmic reticulum organelle imaged by ER-Tracker™ Blue White DPX dye staining (Ex. LED 365 nm) (shown in light blue color), and mitochondrial visualization by MitoView™ Green (Ex. LED 470 nm) staining (shown in green color). **(A)** Images acquired after 5 days of incubation with 10 µM RA and in FBS-free serum for 24 h; **(B)** Images after 1 µM Tunicamycin (ER stress inducer) treatment for 5 h; and **(C)** after 1 µM TUN incubation for 5 h and 24 h treatment with curcumin, fish oil, and BDNF-loaded LCNPs (MO/FO/CU/BDNF) (see the treatment protocol depicted in Fig. 8, bottom row scheme). Scale bar: 15 µm.

LCNPs for 48 h. The live cells were quantified indirectly by the lactate dehydrogenase activity in the cytoplasm of intact cells, which were lysed to release the present LDH protein. The results obtained with the LDH assay (Fig. 7) demonstrated that there is no significant difference (**$p < 0.01$) between the dead cells after treatment with blank (MO) LCNPs and the dead cells in the control (RA(−)FBS or starved cells). At variance, a significant decrease of dead cells was observed upon treatment with all BDNF-loaded LCNPs as compared to the dead cell control. A significant increase (##$p < 0.01$) of the live cells was determined upon treatment with FO- and BDNF-loaded LCNPs as compared to the live cell control (RA(−)FBS or starved cells). A trend of increasing live cells was observed with CU-, FO-, and BDNF-loaded LCNPs. This corroborates with the fact that PUFAs, in a combination with liquid crystalline monoolein (MO)-based nano-assembles, exert a real potentiation effect on the neurotrophic factor protein BDNF [45,80].

The obtained data show that BDNF-loaded LCNPs are safe and favor cellular survival and the protection against cell death induced by serum starvation. In fact, serum provides optimal conditions for cell growth and its deprivation induces cellular apoptosis. Therefore, one can consider the regenerative potential of the BDNF-loaded LCNPs against cellular apoptosis induced by neurotrophin deficiency.

In summary, the results from both the MTT and LDH cytotoxicity assays evidenced that the single- or multidrug-loaded liquid crystalline nanoparticles, containing neurotrophin BDNF, are safe and contribute to cellular repair via protection from cell death.

3.3. *Cellular model of tunicamycin neurotoxicity and tunicamycin-induced ER stress*

Fig. 8 summarizes the cellular treatment schemes employed here to study the tunicamycin cytotoxicity and the tunicamycin-induced ER stress in differentiated human neuroblastoma SH-SY5Y cells as a mechanism of neurodegeneration. Tunicamycin-induced ER stress will be quantified by the fluorescence of Thioflavin T (ThT). The ThT dye (4-(3,6-dimethyl-1,3-benzothiazol-3-ium-2-yl)-N,N-dimethylaniline chloride) binds to protein aggregates and exhibits enhanced fluorescence, which is proportional to the ER stress [95–99].

3.3.1. *Cytotoxicity of tunicamycin to differentiated SH-SY5Y cells*

The human neuroblastoma SH-SY5Y cells were seeded and differentiated by retinoic acid RA (10 µM) for 5 days and deprived of FBS for 24 h. To establish the optimal concentration of the ER stress inducer

tunicamycin (TUN), that causes perceptible death in RA-differentiated SH-SY5Y cells, the cells were treated with different concentrations of the TUN compound for 24 h (Fig. 9). To visually monitor the changes in the cellular morphology and viability, optical micrographs were recorded following the exposure of the RA-differentiated SH-SY5Y cells to TUN (0–10 μM). Fig. 9A shows the adherent control cells which developed elongated neurites at no tunicamycin treatment (0 μM). The elongated cells tended to evolve towards more rounded shapes upon deprivation from serum (FBS). About half of the cells transformed into more rounded shapes and the length of their neurites decreased upon the exposure to TUN (1 μM). The detected cell detachment was indicative for the onset of the apoptotic and/or cell death process. The cell exposure to 10 μM TUN concentration, which mimics an acute stress condition, revealed a massive cell death with cell confluence decreasing to <5% (Fig. 9A).

The concentration of tunicamycin inducing the cellular stress was quantitatively determined by a MTT test (Fig. 9B). The toxicity of TUN to RA-differentiated SH-SY5Y cells was studied at increasing concentrations from 0 to 50 μM (top row scheme in Fig. 8). The results showed a dose-dependent decrease in the cellular viability *versus* TUN concentration. A 50% decrease in cell viability was established at TUN concentrations between 0.5 and 1 μM. Higher concentrations (10–50 μM) caused massive cell death in the samples. Similar results were obtained by Zamarbide et al. for human neuroblastoma SH-SY5H cells death measured by the activity of released LDH in culture medium [91]. Based on these data, a concentration of 1 μM of tunicamycin (TUN) for 5 h and a concentration of 2.5 μM of LCNPs loaded with BDNF were determined for the subsequent experiments.

3.3.2. *Changes in cellular morphology and viability upon multidrug-loaded LCNPs treatment of a tunicamycin-induced ER stress model*

Tunicamycin cytotoxicity is expected to induce ER stress and to lead to neuronal cell death in human neuroblastoma SH-SY5Y cells differentiated by retinoic acid and deprived of fetal bovine serum (FBS). TUN treatment can be followed by abnormal accumulation and aggregation of disease-specific proteins in addition to the oxidative stress and cellular apoptosis effects provoked by serum starvation. Here we investigate whether single- or multidrug-loaded LCNPs (fish oil, curcumin, BDNF) can protect from ER stress-induced neuronal cell damage and promote neuronal survival. To assess the effects of the LCNPs in RA-differentiated SH-SY5Y cells stressed by tunicamycin, images of the samples were acquired by fluorescence microscopy (Fig. 10) and the fluorescence intensity was quantitatively analyzed. The fluorescence microscopy imaging allowed determining the subcellular localization of the ThT staining in the cells treated by 1 μM TUN for 5 h. The ThT fluorescence was co-localized with that of the ER-tracker in the perinuclear region of the tunicamycin-treated cells.

The DIC micrograph in Fig. 10A(top row) shows the morphology of control cells (RA(−)FBS - SH-SY5Y). A lot of cells deprived from serum were still attached to the plate and a few cells were in an apoptotic state. The cellular endoplasmic reticulum and mitochondria organelles were stained by ER-Tracker™ Blue and MitoView™ Green dyes (Fig. 10A, middle and bottom panels). The DIC micrograph in Fig. 10B(top) shows the morphology of the cells exposed to ER-inducer tunicamycin (1 μM) for 5 h. Living cells with extended neurites are attached to the surface, but several other cells are in a necrotic state. The fluorescent images of the stained ER and mitochondria organelles demonstrate the distortions in the sub-cellular organelle network in the TUN-treated cells (Fig. 10B, middle and bottom panels). The DIC micrograph in Fig. 10C shows the morphology of the cells treated by (MO/FO/CU/BDNF) LCNPs for 24 h after exposure to TUN (1 μM) during 5 h. Markedly, cell survival effects and growth of neurites extensions were observed. The images of the stained ER and mitochondria (Fig. 10C) indicated a recovery of the morphologies similarly to the living cells controls. Recent studies have suggested the implication of the PI3/Akt/GSK3 and PI3/Akt/CREB/BDNF signaling pathways in the neuroprotective activity of curcumin and BDNF and the association of these two main pathways with antioxidant,

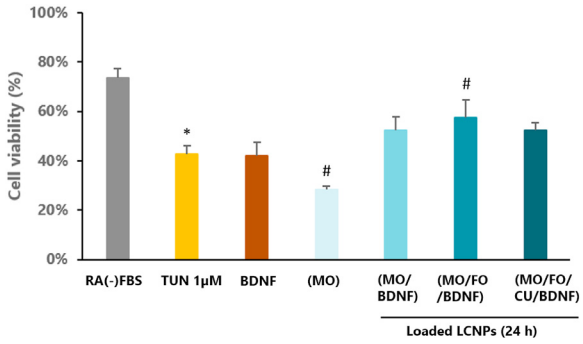

Fig. 11. Cellular viability determined by a MTT assay of RA-differentiated SH-SY5Y subjected to ER stress upon TUN (1 μM) 5 h incubation and treated by blank or multicompound-loaded liquid crystalline nanoparticles (LCNPs) during 24 h. Significant differences were observed with *p < 0.05 *versus* RA(−)FBS control, and #p < 0.05 *versus* tunicamycin (TUN) alone.

anti-inflammatory, anti-apoptosis, and mitochondria biogenesis effects of curcumin [108,111–113]. Such mechanisms can explain the observed here effects. Thus, the performed investigations suggest neuronal cell protection or repair of the TUN-damaged cells by the (MO/FO/-CU/BDNF) LCNPs.

The cellular viabilities were quantified by a MTT assay after cellular exposure to the ER stress-inducer tunicamycin (TUN 1 μM) for 5 h followed by treatment with nanoparticles of different compositions for 24 h (Fig. 11). At a lipid concentration of 2.5 μM, the LCNPs were loaded by BDNF (5 ng/ml). The results presented in Fig. 11 indicate a significant decrease (*p < 0.05) of cell viability upon tunicamycin treatment (43 ± 3.1%) as compared to the cell viability of starved cells (RA(−)FBS), which was equal to 74 ± 3.7%. For TUN (1 μM)-damaged cells, a significant decrease (#p < 0.05) of cell viability was observed with BDNF-free and non-loaded (MO) LCNPs. However, a trend of increasing cellular viability was established for both single BDNF-loaded LCNPs and multi-loaded (MO/FO/CU/BDNF) LCNPs. Fig. 11 demonstrates the significant increase (#p < 0.05) of the cellular viability observed with the FO/BDNF-loaded LCNPs (57 ± 7.0%). From these results, we can suggest that the BDNF-loaded LCNPs promote the cellular survival upon TUN-induced ER stress that provokes cell death.

3.4. *Neuroprotective effects of BDNF-loaded LCNPs in ER stress cellular model*

The neuroprotective effects of BDNF-loaded LCNPs against the endoplasmic reticulum (ER) stress, which is one of the risk factors for neurodegenerative disorders, was studied in the tunicamycin-induced ER stress model. As an inhibitor of N-glycosylation and proper protein folding, tunicamycin promotes unfolded or misfolded proteins to accumulate in the ER compartment thus causing ER stress. We exploited the fact that the dye Thioflavin T (ThT) selectively binds to generated protein aggregates and reveals their presence through its enhanced fluorescence intensity [95–99]. We analyzed the changes in the ThT fluorescence in co-localization studies with the ER organelle in order to evaluate the neuroprotective properties of the studied LCNPs.

3.4.1. *Quantification of endoplasmic reticulum stress after treatment with BDNF-loaded LCNPs*

The ER stress model induced using RA-differentiated human neuroblastoma SH-SY5Y cells was validated by the increased fluorescence of Thioflavin T after TUN treatment. For this purpose, ThT (5 μM) was added to the cultures in the presence of the ER stress-inducing agent (1 μM TUN) (Fig. 12). We determined the subcellular localization of the ThT staining in RA-differentiated SH-SY5Y cells treated with 1 μM TUN for 5 h. The microscopy images (Fig. 12A) show the fluorescence pattern of the ER tracker, which is visualized in the perinuclear region of the TUN-

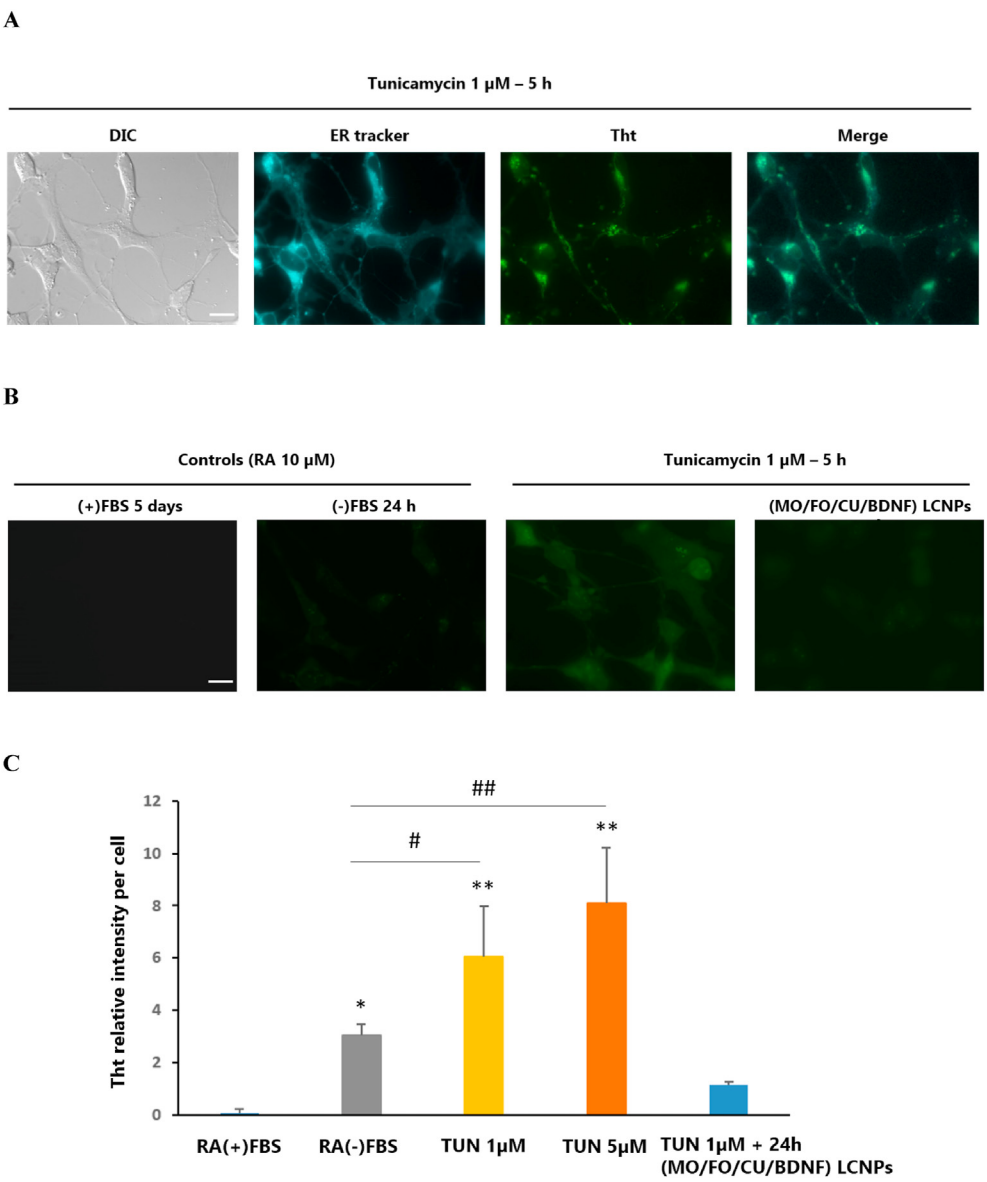

Fig. 12. ThT fluorescence in retinoic acid (RA)-differentiated human SH-SY5Y cells in the presence of the ER-stress inducer tunicamycin (TUN). The cells were treated with 1 or 5 µM TUN for 5 h. **A)** Images revealing co-localization of Thioflavine T (ThT) and ER tracker fluorescence in cells treated with TUN. The cells were stained with 5 µM ThT and ER tracker before imaging by a ZEISS microscope (n = 2). Scale bar: 15 µm. **B)** Living cell images acquired with treatment with CU- and BDNF-loaded LCNPs *versus* controls. Scale bar: 15 µm. **C)** Fluorescence intensity quantification histograms. A significant increase in fluorescence is observed with TUN-treated cells: *$p < 0.05$ and **$p < 0.01$ *versus* RA(+)FBS cells; #$p < 0.05$ and ##$p < 0.01$ *versus* RA(−)FBS cells. A significant decrease in fluorescence is observed with (MO/FO/CU/BDNF) LCNPs treatment as compared to TUN (1 or 5 µM). Scale bar: 15 µm.

treated cells. The ThT fluorescence was colocalized with the ER tracker staining (Fig. 12A). This result is consistent with the fact that ThT did interact with the misfolded protein aggregates produced in the endoplasmic reticulum of the TUN-treated cells.

The ThT fluorescence intensity was investigated in RA-differentiated human neuroblastoma SH-SY5Y cells, which were cultured in the absence (controls) or in the presence of 1 or 5 µM tunicamycin ER-stress inducer. After exposure to TUN for 5 h, the cells were treated with curcumin, fish oil and BDNF-loaded liquid crystalline nanoparticles (MO/FO/CU/BDNF) LCNPs for 24 h at 5 µM lipid concentration (Fig. 12B and C). The fluorescence images in Fig. 12B show a low-intensity ThT fluorescence in the absence of TUN. The ThT fluorescence was enhanced in the cells exposed to the ER stress inducer. However, the ThT fluorescence diminished in the TUN-stressed cells, which were treated by multicompound-loaded nanoparticles (MO/FO/CU/BDNF) LCNPs.

Quantitative results were obtained after image analysis with the *ImageJ* software. Fig. 12C shows that ThT fluorescence intensity was significantly enhanced in the tunicamycin-treated cells relative to controls. An essential difference in the fluorescence intensity was observed in the presence of 1 µM Tunicamycin (6-fold, **$p < 0.01$ compared to the RA(+)FBS condition and 2-fold, #$p < 0.05$ compared to the RA(−)FBS condition). Moreover, a significant intensity increase ($p < 0.01$) was determined upon augmenting the TUN concentration to 5 µM as compared to the non-stressed cells (RA with or without FBS).

The fluorescence intensity in cells treated by FO/CU/BDNF-loaded LCNPs was not significantly different as compared to the non-stressed cells (RA with or without FBS) (Fig. 12C). However, the ThT fluorescence significantly decreased when the cells, which were first exposed to the ER-stress inducer (TUN), were subsequently treated by the (MO/FO/CU/BDNF) LCNPs. This result revealed the effect of the LCNPs on the diminution of the tunicamycin-induced ER stress in RA-differentiated human neuroblastoma SH-SY5Y cells. The obtained data validated the designed *in vitro* model of ER stress induced by tunicamycin in RA-differentiated SH-SY5Y cells. Moreover, the combined drug (curcumin, fish oil and BDNF)-loaded LCNPs appeared to be a promising treatment for ER stress diminution under neurodegenerative conditions.

Molecular mechanisms of BDNF-mediated neuroprotection during ER stress response have been proposed by Chen et al. and Shimoke et al. [112,113]. The authors have shown that the pro-apoptotic protein CHOP partially mediates the ER stress-induced neuronal death. BDNF suppresses the ER stress-induced upregulation/nuclear translocation of CHOP. In fact, the transcription of CHOP is regulated by ATF4, ATF6, and

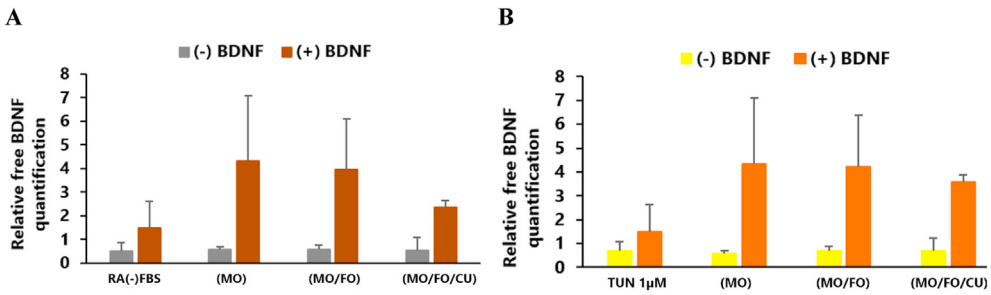

Fig. 13. Concentrations of human free BDNF normalized with regard to the total protein concentration in SH-SY5Y cells treated by: **A)** LCNPs 5 μM during 48 h treatment, and **B)** TUN 1 μM during 5 h and LCNPs 5 μM during 48 h treatment (n = 2).

XBP1; and BDNF selectively blocks the ATF6/CHOP pathway. Furthermore, BDNF inhibits the induction of the death receptor 5 (DR5), a transcriptional target of CHOP [112,113]. Other mechanisms of protection from endoplasmic reticulum stress consider the signaling pathways affected by curcumin and the promotion of the neuronal survival through enhanced BDNF secretion and increased phosphorylation of CREB [105–111].

Based on the above, it can be suggested that the designed (MO/FO/CU/BDNF) LCNPs exert a neuroprotective effect against tunicamycin-induced endoplasmic reticulum stress and may find a potential application towards cellular regeneration in neurodegenerative disorders.

3.4.2. Human free BDNF quantification in RA-differentiated SH-SY5Y cells

We quantitatively determined the concentrations of free brain-derived neurotrophic factor (BDNF) in SH-SY5Y cell supernates by a Quantikine® ELISA Human Free BDNF Immunoassay kit in order to evaluate the capacity of the studied LCNPs to transport neuroprotective molecules into the cells and stimulate the BDNF protein expression after TUN treatment.

The results in Fig. 13 show very low BDNF concentrations in supernates of control differentiated RA(−)FBS SH-SY5Y cells and of cells exposed to tunicamycin (TUN) or treated by blank LCNPs (non-loaded by BDNF). At variance, we observed a trend of increasing BDNF concentrations in cells treated with FO-loaded and BDNF-loaded LCNPs. This increase was higher for the single and dual FO/BDNF-loaded LCNPs with regard to BDNF treatment alone. The obtained results evidenced the capacity of the studied LCNPs to transport the protein drug across the cellular membrane. The multi-loaded (MO/FO/CU/BDNF) LCNPs should be further studied for eventual competition effects for the BDNF loading as well as for the possibly slower kinetics of release of the bioactive curcumin ingredient from the nanoparticles.

4. Conclusion

Lipid-based cubosome and spongosome liquid crystalline nanoparticles involve 3D network architectures of internal compartments, which represent a structural advantage enabling their high encapsulation efficacy for hydrophobic and hydrophilic molecules. These nanoparticles can serve as mesoporous reservoirs for co-encapsulation of neuroprotective ω-3 PUFA-rich fish oil with water-insoluble antioxidants, nutraceuticals, and hydrophilic biomacromolecules toward development of combination treatments against neurodenegeneration. In this work, single-, dual- and multi-loaded nanocarriers of the cubosome or spongosome type were designed by self-assembly. The obtained SAXS results indicated that curcumin (a hydrophobic phytochemical compound) stabilizes the formation of the cubosome nanoparticles. In the dispersions of MO/FO/CU compositions, the curcumin-loaded nanocarriers were found to be of higher inner crystalline order as compared to the LCNPs lacking curcumin. However, the morphological investigation of the dispersed LCNPs established that the co-encapsulated compounds with neuroprotective properties may separate into domains, which is likely due to their limited solubility.

The MO/FO-based nanoparticles were not toxic and delivered the bioactive small molecules and the neurotrophic protein BDNF inside the neuronally derived SH-SY5Y cells subjected to endoplasmic reticulum (ER) stress. The inclusion of fish oil within the liquid crystalline nanoassembles promoted the potentiation of the BDNF activity in the investigated *in vitro* cellular model of neurodegeneration. The cubosomal nanoarchitectures preserved the encapsulated antioxidant and protein molecules in a functional state, ensuring the cellular defense against ER stress. We suggest that the modulation of the ER stress by multidrug-loaded liquid crystalline lipid nanoparticles can be considered as a therapeutic opportunity for neuroprotection and prevention of neurodegeneration. Further studies will be needed in order to determine an eventual synergistic or competitive effect of curcumin and BDNF upon dual delivery by LCNPs aiming at recovery from ER stress and halting neuronal cell death. Low doses of curcumin help enhancing the expression of the neurotrophic factor BDNF. However, the co-administration of the two compounds (CU and BDNF) seems to result in dose-dependent responses, which may lead to attenuation of the survival effects at increased doses.

CRediT authorship contribution statement

Miora Rakotoarisoa: Investigation, Data curation, Writing – original draft. **Borislav Angelov:** Investigation, Formal analysis, Resources, Writing – review & editing. **Markus Drechsler:** Investigation, Visualization. **Valérie Nicolas:** Methodology, Visualization. **Thomas Bizien:** Software, Visualization. **Yulia E. Gorshkova:** Resources. **Yuru Deng:** Resources. **Angelina Angelova:** Conceptualization, Investigation, Methodology, Formal analysis, Writing – original draft, Writing – review & editing, Supervision.

Declaration of competing interest

The authors declare that they have no known competing financial interests or personal relationships that could have appeared to influence the work reported in this paper.

Acknowledgements

The performed research was funded by the "IDI 2017" project of the IDEX Paris-Saclay/ANR-11-IDEX-0003-02 and the projects “Structural Dynamics of Biomolecular Systems” (ELIBIO) (CZ.02.1.01/0.0/0.0/15_003/0000447) and “Advanced research using high-intensity laser produced photons and particles” (CZ.02.1.01/0.0/0.0/16_019/0000789) from the European Regional Development Fund. B.A. obtained also a financial support from the collaborative international project with JINR, Dubna (3+3 program, No. 204, item 27 from 25.03.2020). Y.D. was supported by grants from the Wenzhou Institute, University of Chinese Academy of Sciences (Grant No. WIUCASQD2019005) and the National Natural Science Foundation of China (Grant No: 31670841). We gratefully acknowledge the allocation of beam time at Synchrotron

SOLEIL (Saint Aubin, France) through the projects 20181489, 20201321, and 20210580 and all scientific and technical support at the SWING beamline. M.D. is supported by the collaborative research center SFB840 of the German Science Foundation DFG. AA acknowledges a membership in CNRS GDR2088 BIOMIM research network.

References

[1] J.L. Cummings, T. Morstorf, K. Zhong, Alzheimer's disease drug-development pipeline: few candidates, frequent failures, Alzheimer's Res. Ther. 6 (2014) 37, https://doi.org/10.1186/alzrt269.
[2] I.G. Onyango, J.P. Bennett, G.B. Stokin, Regulation of neuronal bioenergetics as a therapeutic strategy in neurodegenerative diseases, Neural. Regen. Res. 16 (8) (2021) 1467–1482, https://doi.org/10.4103/1673-5374.303007.
[3] H. Prentice, J.P. Modi, J.Y. Wu, Mechanisms of neuronal protection against excitotoxicity, endoplasmic reticulum stress, and mitochondrial dysfunction in stroke and neurodegenerative diseases, Oxid. Med. Cell. Longev. (2015) 964518, https://doi.org/10.1155/2015/964518 (2015).
[4] R. Cascella, C. Cecchi, Calcium dyshomeostasis in Alzheimer's disease pathogenesis, Int. J. Mol. Sci. 22 (9) (2021) 4914, https://doi.org/10.3390/ijms22094914.
[5] P. Pantiya, C. Thonusin, N. Chattipakorn, S.C. Chattipakorn, Mitochondrial abnormalities in neurodegenerative models and possible interventions: focus on Alzheimer's disease, Parkinson's disease, Huntington's disease, Mitochondrion 55 (2020) 14–47, https://doi.org/10.1016/j.mito.2020.08.003.
[6] G. Monzio Compagnoni, A. Di Fonzo, S. Corti, G.P. Comi, N. Bresolin, E. Masliah, The role of mitochondria in neurodegenerative diseases: the lesson from Alzheimer's disease and Parkinson's disease, Mol. Neurobiol. 57 (2020) 2959–2980, https://doi.org/10.1007/s12035-020-01926-1.
[7] M. Akbar, et al., Mitochondrial dysfunction and cell death in neurodegenerative diseases through nitroxidative stress, Brain Res 1637 (2016) 34–55, https://doi.org/10.1016/j.brainres.2016.02.016.
[8] M. Karbowski, A. Neutzner, Neurodegeneration as a consequence of failed mitochondrial maintenance, Acta Neuropathol 123 (2) (2012) 157–171, https://doi.org/10.1007/s00401-011-0921-0.
[9] S.D. Chen, C.L. Wu, W.C. Hwang, D.I. Yang, More insight into BDNF against neurodegeneration: anti-apoptosis, anti-oxidation, and suppression of autophagy, Int. J. Mol. Sci. 18 (2017) 545, https://doi.org/10.3390/ijms18030545.
[10] M. Miranda, J.F. Morici, M.B. Zanoni, P. Bekinschtein, Brain-derived neurotrophic factor: a key molecule for memory in the healthy and the pathological brain, Front. Cell. Neurosci. 13 (2019) 363, https://doi.org/10.3389/fncel.2019.00363.
[11] M. Mitre, A. Mariga, M.V. Chao, Neurotrophin signalling: novel insights into mechanisms and pathophysiology, Clin. Sci. 131 (2017) 13–23, https://doi.org/10.1042/CS20160044.
[12] P. Kowianski, G. Lietzau, E. Czuba, M. Waskow, A. Steliga, J. Morys, BDNF: a key factor with multipotent impact on brain signaling and synaptic plasticity, Cell. Mol. Neurobiol. 38 (2018) 579–593, https://doi.org/10.1007/s10571-017-0510-4.
[13] S.H. Choi, E. Bylykbashi, Z.K. Chatila, S.W. Lee, B. Pulli, G.D. Clemenson, et al., Combined adult neurogenesis and BDNF mimic exercise effects on cognition in an Alzheimer's mouse model, Science 361 (2018) eaan8821, https://doi.org/10.1126/science.aan8821.
[14] M.A. Rather, A. Khan, S. Alshahrani, H. Rashid, M. Qadri, S. Rashid, et al., Inflammation and Alzheimer's disease: mechanisms and therapeutic implications by natural products, Mediat. Inflamm. 2021 (2021) 9982954, https://doi.org/10.1155/2021/9982954.
[15] N.T. Sprenkle, S.G. Sims, C.L. Sánchez, G.P. Meares, Endoplasmic reticulum stress and inflammation in the central nervous system, Mol. Neurodegener. 12 (1) (2017) 42, https://doi.org/10.1186/s13024-017-0183-y.
[16] C.G. Glabe, R. Kayed, Common structure and toxic function of amyloid oligomers implies a common mechanism of pathogenesis, Neurology 66 (2) (2006) S74–S78, https://doi.org/10.1212/01.wnl.0000192103.24796.42.
[17] W.W. Smith, H. Jiang, Z. Pei, Y. Tanaka, H. Morita, A. Sawa, et al., Endoplasmic reticulum stress and mitochondrial cell death pathways mediate A53T mutant alpha-synuclein-induced toxicity, Hum. Mol. Genet. 14 (2005) 3801–3811, https://doi.org/10.1093/hmg/ddi396.
[18] M.T. Herrero, M. Morelli, Multiple mechanisms of neurodegeneration and progression, Prog Neurobiol. 155 (2017) 1–2, https://doi.org/10.1016/j.pneurobio.2017.06.001.
[19] I.G. Onyango, J. Dennis, S.M. Khan, Mitochondrial dysfunction in Alzheimer's disease and the rationale for bioenergetics based therapies, Aging Dis. 7 (2) (2016) 201–214, https://doi.org/10.14336/AD.2015.1007.
[20] Y. Gerakis, C. Hetz, Emerging roles of ER stress in the etiology and pathogenesis of Alzheimer's disease, FEBS J 285 (2018) 995–1011, https://doi.org/10.1111/febs.14332.
[21] T. Shacham, N. Sharma, G.Z. Lederkremer, Protein misfolding and ER stress in Huntington's disease, Front. Mol. Biosci. 6 (2019) 20, https://doi.org/10.3389/fmolb.2019.00020.
[22] R.J.S. Viana, A.F. Nunes, C.M.P. Rodrigues, Endoplasmic reticulum enrollment in Alzheimer's disease, Mol. Neurobiol. 46 (2) (2012) 522–534, https://doi.org/10.1007/s12035-012-8301-x.
[23] K. Endres, S. Reinhardt, ER-stress in Alzheimer's disease: turning the scale? Am. J. Neurodegener. Dis. 2 (2013) 247–265.
[24] W. Paschen, T. Mengesdorf, Endoplasmic reticulum stress response and neurodegeneration, Cell Calcium 38 (2005) 409–415, https://doi.org/10.1016/j.ceca.2005.06.019.
[25] D.I. Briggs, E. Defensor, P.M. Ardestani, B. Yi, M. Halpain, G. Seabrook, M. Shamloo, Role of endoplasmic reticulum stress in learning and memory impairment and Alzheimer's disease-like nuropathology in the PS19 and APPSwe mouse models of tauopathy and amyloidosis, eNeuro 4 (4) (2017), https://doi.org/10.1523/ENEURO.0025-17.2017. ENEURO.0025-17.2017.
[26] R. Vidal, B. Caballero, A. Couve, C. Hetz, Converging pathways in the occurrence of endoplasmic reticulum (ER) stress in Huntington's disease, Curr. Mol. Med. 11 (2011) 1–12, https://doi.org/10.2174/156652411794474419.
[27] B.J. Turner, J.D. Atkin, ER stress and UPR in familial amyotrophic lateral sclerosis, Curr. Mol. Med. 6 (2006) 79–86, https://doi.org/10.2174/156652406775574550.
[28] W. Paschen, Endoplasmic reticulum dysfunction in brain pathology: critical role of protein synthesis, Curr. Neurovascular Res. 1 (2) (2004) 173–181, https://doi.org/10.2174/1567202043480125.
[29] W. Scheper, J.J. Hoozemans, Endoplasmic reticulum protein quality control in neurodegenerative disease: the good, the bad and the therapy, Curr. Med. Chem. 16 (5) (2009) 615–626, https://doi.org/10.2174/092986709787458506.
[30] N. Ogen-Shtern, T. Ben David, G.Z. Lederkremer, Protein aggregation and ER stress, Brain Res. 1648 (Pt B) (2016) 658–666, https://doi.org/10.1016/j.brainres.2016.03.044.
[31] C. Hetz, S. Saxena, ER stress and the unfolded protein response in neurodegeneration, Nat. Rev. Neurol. 13 (2017) 477–491, https://doi.org/10.1038/nrneurol.2017.99.
[32] V.H. Cornejo, C. Hetz, The unfolded protein response in Alzheimer's disease, Semin. Immunopathol. 35 (3) (2013) 277–292, https://doi.org/10.1007/s00281-013-0373-9.
[33] T.K. Chang, D.A. Laurence, M. Lu, J. Tan, J.M. Harnoss, S.A. Marsters, et al., Coordination between two branches of the unfolded protein response determines apoptotic cell fate, Mol. Cell 71 (2018) 629–636, https://doi.org/10.1016/j.molcel.2018.06.038.
[34] C. Hetz, F.R. Papa, The unfolded protein response and cell fate control, Mol. Cell 69 (2018) 169–181, https://doi.org/10.1016/j.molcel.2017.06.017.
[35] C. Hetz, E. Chevet, H.P. Harding, Targeting the unfolded protein response in disease, Nat. Rev. Drug Discov. 12 (9) (2013) 703–719, https://doi.org/10.1038/nrd3976.
[36] T. Katayama, K. Imaizumi, T. Manabe, J. Hitomi, T. Kudo, M. Tohyama, Induction of neuronal death by ER stress in Alzheimer's disease, J. Chem. Neuroanat. 28 (2004) 67–78, https://doi.org/10.1016/j.jchemneu.2003.12.004.
[37] S. Tajiri, S. Oyadomari, S. Yano, M. Morioka, T. Gotoh, J.I. Hamada, Y. Ushio, M. Mori, Ischemia-induced neuronal cell death is mediated by the endoplasmic reticulum stress pathway involving CHOP, Cell Death Differ 11 (2004) 403–415, https://doi.org/10.1038/sj.cdd.4401365.
[38] S.E. Logue, P. Cleary, S. Saveljeva, A. Samali, New directions in ER stress-induced cell death, Apoptosis 18 (2013) 537–546, https://doi.org/10.1007/s10495-013-0818-6.
[39] T.T. Nguyen, T.T. Dung Nguyen, T.K. Vo, N.M. Tran, M.K. Nguyen, T. Van Vo, G. Van Vo, Nanotechnology-based drug delivery for central nervous system disorders, Biomed. Pharmacother. 143 (2021) 112117, https://doi.org/10.1016/j.biopha.2021.112117.
[40] K. Jagaran, M. Singh, Nanomedicine for neurodegenerative disorders: focus on Alzheimer's and Parkinson's diseases, Int. J. Mol. Sci. 22 (2021) 9082, https://doi.org/10.3390/ijms22169082.
[41] T.B. Soares, L. Loureiro, A.P. Carvalho, M.E.C.R. Oliveira, A. Dias, B. Sarmento, M. Lúcio, Lipid nanocarriers loaded with natural compounds: potential new therapies for age related neurodegenerative diseases? Prog. Neurobiol. 168 (2018) 21–41, https://doi.org/10.1016/j.pneurobio.2018.04.004.
[42] L.F. González, L.E. Bevilacqua, R. Naves, Nanotechnology-based drug delivery strategies to repair the mitochondrial function in neuroinflammatory and neurodegenerative diseases, Pharmaceutics 13 (2021) 2055, https://doi.org/10.3390/pharmaceutics13122055.
[43] A. Angelova, M. Drechsler, V.M. Garamus, B. Angelov, Liquid crystalline nanostructures as PEGylated reservoirs of omega-3 polyunsaturated fatty acids: structural insights toward delivery formulations against neurodegenerative disorders, ACS Omega 3 (2018) 3235–3247, https://doi.org/10.1021/acsomega.7b01935.
[44] C. Martinelli, C. Pucci, M. Battaglini, A. Marino, G. Ciofani, Antioxidants and nanotechnology: promises and limits of potentially disruptive approaches in the treatment of central nervous system diseases, Adv. Healthc. Mater. 9 (3) (2020) 1901589, https://doi.org/10.1002/adhm.201901589.
[45] A. Angelova, B. Angelov, Dual and multi-drug delivery nanoparticles towards neuronal survival and synaptic repair, Neural. Regener. Res. 12 (2017) 886–889, https://doi.org/10.4103/1673-5374.208546.
[46] M. Rakotoarisoa, B. Angelov, V.M. Garamus, A. Angelova, Curcumin- and fish oil-loaded spongosome and cubosome nanoparticles with neuroprotective potential against H_2O_2-induced oxidative stress in differentiated human SH-SY5Y cells, ACS Omega 4 (2019) 3061–3073, https://doi.org/10.1021/acsomega.8b03101.
[47] M. Rakotoarisoa, B. Angelov, S. Espinoza, K. Khakurel, T. Bizien, A. Angelova, Cubic liquid crystalline nanostructures involving catalase and curcumin: BioSAXS study and catalase peroxidatic function after cubosomal nanoparticle treatment of differentiated SH-SY5Y cells, Molecules 24 (2019) E3058, https://doi.org/10.3390/molecules24173058.
[48] A. Angelova, M. Drechsler, V.M. Garamus, B. Angelov, Pep-lipid cubosomes and vesicles compartmentalized by micelles from self-assembly of multiple

neuroprotective building blocks including a large peptide hormone PACAP-DHA, ChemNanoMat 5 (2019) 1381–1389, https://doi.org/10.1002/cnma.201900468.
[49] L.P.B. Guerzoni, V. Nicolas, A. Angelova, In vitro modulation of TrkB receptor signaling upon sequential delivery of curcumin-DHA loaded carriers towards promoting neuronal survival, Pharmaceut. Res. 34 (2017) 492–505, https://doi.org/10.1007/s11095-016-2080-4.
[50] A. Yaghmur, G. Glatter, Characterization and potential applications of nanostructured aqueous dispersions, Adv. Colloid Interface Sci. 147–148 (2009) 333–342, https://doi.org/10.1016/j.cis.2008.07.007.
[51] V. Alfredsson, P. Lo Nostro, B. Ninham, T. Nylander, Morphologies and structure of brain lipid membrane dispersions, Front. Cell Dev. Biol. 9 (2021) 675140, https://doi.org/10.3389/fcell.2021.675140.
[52] A. Chemelli, B. Conde-Valentín, F. Uhlig, O. Glatter, Amino acid induced modification of self-assembled monoglyceride-based nanostructures, Langmuir 31 (2015) 10377–10381, https://doi.org/10.1021/acs.langmuir.5b02139.
[53] J. Zhai, B. Fan, S.H. Thang, C.J. Drummond, Novel amphiphilic block copolymers for the formation of stimuli-responsive non-lamellar lipid nanoparticles, Molecules 26 (2021) 23648, https://doi.org/10.3390/molecules26123648.
[54] A.R. Faria, O.F. Silvestre, C. Maibohm, R.M.R. Adão, B.F.B. Silva, J.B. Nieder, Cubosome nanoparticles for enhanced delivery of mitochondria anticancer drug elesclomol and therapeutic monitoring via sub-cellular NAD(P)H multi-photon fluorescence lifetime imaging, Nano Res 12 (2019) 991–998, https://doi.org/10.1007/s12274-018-2231-5.
[55] H. Wu, J. Li, Q. Zhang, X. Yan, L. Guo, X. Gao, M. Qiu, et al., A novel small Odorranalectin-bearing cubosomes: preparation, brain delivery and pharmacodynamic study on amyloid-β_{25-35}-treated rats following intranasal administration, Eur. J. Pharm. Biopharm. 80 (2012) 368–378, https://doi.org/10.1016/j.ejpb.2011.10.012.
[56] H. Azhari, M. Younus, S.M. Hook, B.J. Boyd, S.B. Rizwan, Cubosomes enhance drug permeability across the blood-brain barrier in zebrafish, Int. J. Pharm. 600 (2021) 120411, https://doi.org/10.1016/j.ijpharm.2021.120411.
[57] M. Rakotoarisoa, A. Angelova, Amphiphilic nanocarrier systems for curcumin delivery in neurodegenerative disorders, Medicines 5 (2018) 126, https://doi.org/10.3390/medicines5040126.
[58] Y. Mohammad, R.N. Prentice, B.J. Boyd, S.B. Rizwan, Comparison of cubosomes and hexosomes for the delivery of phenytoin to the brain, J. Colloid Interface Sci. 605 (2022) 146–154, https://doi.org/10.1016/j.jcis.2021.07.070.
[59] A. Angelova, B. Angelov, M. Drechsler, T. Bizien, Y.E. Gorshkova, Y. Deng, Plasmalogen-based liquid crystalline multiphase structures involving docosapentaenoyl derivatives inspired by biological cubic membranes, Front. Cell Dev. Biol. 9 (2021) 617984, https://doi.org/10.3389/fcell.2021.617984.
[60] J. Zhai, C. Fong, N. Tran, C.J. Drummond, Non-lamellar lyotropic liquid crystalline lipid nanoparticles for the next generation of nanomedicine, ACS Nano 13 (2019) 6178–6206, https://doi.org/10.1021/ACSNANO.8B07961.
[61] A. Yaghmur, H. Mu, Recent advances in drug delivery applications of cubosomes, hexosomes, and solid lipid nanoparticles, Acta Pharm. Sin. B 11 (2021) 871–885, https://doi.org/10.1016/j.apsb.2021.02.013.
[62] A.M. Mohsen, M.M. Younis, A. Salama, A.B. Darwish, Cubosomes as a potential oral drug delivery system for enhancing the hepatoprotective effect of coenzyme Q10, J. Pharmaceut. Sci. 110 (7) (2021) 2677–2686, https://doi.org/10.1016/j.xphs.2021.02.007.
[63] Z. Liu, L. Yu, P. Gu, R. Bo, S. Xu, A. Wusiman, J. Liu, Y. Hu, D. Wang, Surface-engineered cubosomes serve as a novel vaccine adjuvant to modulate innate immunity and improve adaptive immunity in vivo, Int. J. Nanomed. 15 (2020) 8595–8608, https://doi.org/10.2147/IJN.S266165.
[64] C.V. Kulkarni, V.K. Vishwapathi, A. Quarshie, Z. Moinuddin, J. Page, P. Kendrekar, S.S. Mashele, Self-assembled lipid cubic phase and cubosomes for the delivery of a model drug (aspirin), Langmuir 33 (2017) 9907–9915, https://doi.org/10.1021/acs.langmuir.7b02486.
[65] H. Scharfman, J. Goodman, A. Macleod, S. Phani, C. Antonelli, S. Croll, Increased neurogenesis and the ectopic granule cells after intrahippocampal BDNF infusion in adult rats, Exp. Neurol. 192 (2) (2005) 348–356, https://doi.org/10.1016/j.expneurol.2004.11.016.
[66] T. Zigova, V. Pencea, S.J. Wiegand, M.B. Luskin, Intraventricular administration of BDNF increases the number of newly generated neurons in the adult olfactory bulb, Mol. Cell. Neurosci. 11 (1998) 234–245, https://doi.org/10.1006/mcne.1998.0684.
[67] T. Numakawa, H. Odaka, N. Adachi, Actions of brain-derived neurotrophin factor in the neurogenesis and neuronal function, and its involvement in the pathophysiology of brain diseases, Int. J. Mol. Sci. 19 (2018) 3650, https://doi.org/10.3390/ijms19113650.
[68] E. Palasz, A. Wysocka, A. Gasiorowska, M. Chalimoniuk, W. Niewiadomski, G. Niewiadomska, BDNF as a promising therapeutic agent in Parkinson's disease, Int. J. Mol. Sci. 21 (2020) 1170, https://doi.org/10.3390/ijms21031170.
[69] C. Zuccato, M. Marullo, B. Vitali, A. Tarditi, C. Mariotti, M. Valenza, N. Lahiri, et al., Brain-derived neurotrophic factor in patients with Huntington's disease, PLoS One 6 (2011), e22966, https://doi.org/10.1371/journal.pone.0022966.
[70] L. Aron, R. Klein, Repairing the parkinsonian brain with neurotrophic factors, Trends Neurosci. 34 (2) (2011) 88–100, https://doi.org/10.1016/j.tins.2010.11.001.
[71] Y. Jiang, J.M. Fay, C.D. Poon, et al., Nanoformulation of brain-derived neurotrophic factor with target receptor-triggered-release in the central nervous system, Adv. Funct. Mater. 28 (6) (2018) 1703982, https://doi.org/10.1002/adfm.201703982.
[72] C. Faustino, P. Rijo, C.P. Reis, Nanotechnological strategies for nerve growth factor delivery: therapeutic implications in Alzheimer's disease, Pharmacol. Res. 120 (2017) 68–87, https://doi.org/10.1016/j.phrs.2017.03.020.
[73] M. Bu, J. Tang, Y. Wei, Y. Sun, X. Wang, L. Wu, H. Liu, Enhanced bioavailability of nerve growth factor with phytantriol lipid-based crystalline nanoparticles in cochlea, Int. J. Nanomed. 10 (2015) 6879–6889, https://doi.org/10.2147/IJN.S82944.
[74] Y. Xing, C.Y. Wen, S.T. Li, Z.X. Xia, Non-viral liposome-mediated transfer of brain-derived neurotrophic factor across the blood-brain barrier, Neural. Regen. Res. 11 (4) (2016) 617–622, https://doi.org/10.4103/1673-5374.180747.
[75] C.D.F. Lopes, N.P. Goncalves, C.P. Gomes, BDNF gene delivery mediated by neuron-targeted nanoparticles is neuroprotective in peripheral nerve injury, Biomaterials 121 (2017) 83–96, https://doi.org/10.1016/j.biomaterials.2016.12.025.
[76] S. Madduri, B. Gander, Growth factor delivery systems and repair strategies for damaged peripheral nerves, J. Contr. Release 161 (2) (2012) 274–282, https://doi.org/10.1016/j.jconrel.2011.11.036.
[77] N.M. Harris, R. Ritzel, N.S. Mancini, Nanoparticle delivery of brain derived neurotrophic factor after focal cerebral ischemia reduces tissue injury and enhances behavioral recovery, Pharmacol. Biochem. Behav. 150–151 (2016) 48–56, https://doi.org/10.1016/j.pbb.2016.09.003.
[78] M. Bousquet, M. Saint-Pierre, C. Julien, N. Salem, F. Cicchetti, F. Calon, Beneficial effects of dietary omega-3 polyunsaturated fatty acid on toxin-induced neuronal degeneration in an animal model of Parkinson's disease, Faseb. J. 22 (2008) 1213–1225, https://doi.org/10.1096/fj.07-9677com.
[79] Y. Pan, H. Khalil, J. Nicolazzo, The impact of docosahexaenoic acid on Alzheimer's disease: is there a role of the blood-brain barrier? Curr. Clin. Pharmacol. 10 (2015) 222–241, https://doi.org/10.2174/1574884710031508201515 32.
[80] C. Géral, A. Angelova, B. Angelov, V. Nicolas, S. Lesieur, Multicompartment lipid nanocarriers for targeting of cells expressing brain receptors, in: N. Garti, R. Mezzenga, P. Somasundaran (Eds.), Self-Assembled Supramolecular Architectures: Lyotropic Liquid Crystals", John Wiley & Sons, Inc., New Jersey, NJ, USA, 2012, pp. 319–355, https://doi.org/10.1002/9781118336632.ch11.
[81] K. Khezri, M. Saeedi, H. Mohammadamini, A.S. Zakaryaei, A comprehensive review of the therapeutic potential of curcumin nanoformulations, Phytother Res. 35 (2021) 5527–5563, https://doi.org/10.1002/ptr.7190.
[82] S.C. Gupta, S. Patchva, B.B. Aggarwal, Therapeutic roles of curcumin: lessons learned from clinical trials, AAPS J 15 (2013) 195–218, https://doi.org/10.1208/s12248-012-9432-8.
[83] M.M. Serafini, M. Catanzaro, M. Rosini, M. Racchi, C. Lanni, Curcumin in Alzheimer's disease: can we think to new strategies and perspectives for this molecule? Pharmacol. Res. 124 (2017) 146–155, https://doi.org/10.1016/j.phrs.2017.08.004.
[84] R.B. Mythri, M.M.S. Bharath, Curcumin: a potential neuroprotective agent in Parkinson's disease, Curr. Pharmaceut. Des. 18 (2012) 91–99, https://doi.org/10.2174/138161212798918995.
[85] T. Ahmed, A.-H. Gilani, Therapeutic potential of turmeric in Alzheimer's disease: curcumin or curcuminoids? Phytother Res 28 (2013) 517–525, https://doi.org/10.1002/ptr.5030.
[86] N. Brondino, S. Re, A. Boldrini, A. Cuccomarino, N. Lanati, F. Barale, P. Politi, Curcumin as a therapeutic agent in dementia: a mini systematic review of human studies, Sci. World J. (2014) 174282, https://doi.org/10.1155/2014/174282 (2014).
[87] S.M. Nam, J.H. Choi, D.Y. Yoo, W. Kim, H.Y. Junk, J.W. Kim, et al., Effects of curcumin (Curcuma longa) on learning and spatial memory as well as cell proliferation and neuroblast differentiation in adult and aged mice by upregulating brain-derived neurotrophic factor and CREB signaling, J. Med. Food 17 (6) (2014) 641–649, https://doi.org/10.1089/jmf.2013.2965.
[88] J. Wu, Q. Li, X. Wang, S. Yu, L. Li, X. Wu, Y. Chen, et al., Neuroprotection by curcumin in ischemic brain injury involves the Akt/Nrf2 pathway, PLoS One 8 (2013) 59843, https://doi.org/10.1371/journal.pone.0059843.
[89] H. Wang, X. Wang, Z.J. Ke, A.L. Comer, M. Xu, J.A. Frank, Z. Zhang, X. Shi, J. Luo, Tunicamycin-induced unfolded protein response in the developing mouse brain, Toxicol. Appl. Pharmacol. 283 (3) (2015) 157–167, https://doi.org/10.1016/j.taap.2014.12.019.
[90] T. Oda, Y. Kosuge, M. Arakawa, K. Ishige, Y. Ito, Distinct mechanism of cell death is responsible for tunicamycin-induced ER stress in SK-N-SH and SH-SY5Y cells, Neurosci. Res. 60 (2008) 29–39, https://doi.org/10.1016/j.neures.2007.09.005.
[91] M. Zamarbide, E. Martinez-Pinilla, A. Ricobaraza, T. Aragón, R. Franco, M. Pérez, Phenyl acyl acids attenuate the unfolded protein response in tunicamycin-treated neuroblastoma cells, PLoS One 8 (8) (2013), e71082, https://doi.org/10.1371/journal.pone.0071082.
[92] A. Angelova, B. Angelov, V.M. Garamus, M. Drechsler, A vesicle-to-sponge transition via the proliferation of membrane-linking pores in omega-3 polyunsaturated fatty acid-containing lipid assemblies, J. Mol. Liq. 279 (2019) 518–523, https://doi.org/10.1016/j.molliq.2019.01.124.
[93] B. Angelov, A. Angelova, V.M. Garamus, M. Drechsler, et al., Earliest stage of the tetrahedral nanochannel formation in cubosome particles from unilamellar nanovesicles, Langmuir 28 (2012) 16647–16655, https://doi.org/10.1021/la302721n.
[94] M. Rakotoarisoa, B. Angelov, S. Espinoza, K. Khakurel, T. Bizien, M. Drechsler, A. Angelova, Composition-switchable liquid crystalline nanostructures as green formulations of curcumin and fish oil, ACS Sustain. Chem. Eng. 9 (2021) 14821–14835, https://doi.org/10.1021/acssuschemeng.1c04706.

[95] K. Naiki, M. Higuchi, T.T. Hosokawa, Fluorometric determination of amyloid fibrils in vitro using the fluorescent dye, thioflavin T1, Anal. Biochem. 177 (2) (1989) 244–249, https://doi.org/10.1016/0003-2697(89)90046-8.
[96] M. Lindgren, K. Sorgjerd, P. Hammarstrom, Detection and characterization of aggregates, prefibrillar amyloidogenic oligomers, and protofibrils using fluorescence spectroscopy, Biophys. J. 88 (6) (2005) 4200–4212, https://doi.org/10.1529/biophysj.104.049700.
[97] E.M. Sigurdsson, Histological staining of amyloid-beta in mouse brains, Methods Mol. Biol. 299 (2005) 299–308, https://doi.org/10.1385/1-59259-874-9:299.
[98] D.R. Beriault, G.H. Werstuck, Detection and quantification of endoplasmic reticulum stress in living cells using the fluorescent compound, Thioflavin T, Biochim. Biophys. Acta 1833 (2013) 2293–2301, https://doi.org/10.1016/j.bbamcr.2013.05.020.
[99] P. Verwilst, K. Kim, K. Sunwoo, H.R. Kim, C. Kang, J.S. Kim, Revealing protein aggregates under thapsigargin-induced ER stress using an ER-targeted Thioflavin, ACS Sens 4 (2019) 2858–2863, https://doi.org/10.1021/acssensors.9b00568.
[100] B. Salehi, D. Calina, A.O. Docea, N. Koirala, S. Aryal, D. Lombardo, L. Pasqua, et al., Curcumin's nanomedicine formulations for therapeutic application in neurological diseases, J. Clin. Med. 9 (2) (2020) 430, https://doi.org/10.3390/jcm9020430.
[101] Q. Shehzad, A. Rehman, S. Mahdi, M. Zuo, M.A. Khan, A. Ali, et al., Improving the oxidative stability of fish oil nanoemulsions by co-encapsulation with curcumin and resveratrol, Colloids Surf. B Biointerfaces 199 (2021) 111481, https://doi.org/10.1016/j.colsurfb.2020.111481.
[102] T. Jiang, W. Liao, C. Charcosset, Recent advances in encapsulation of curcumin in nanoemulsions: a review of encapsulation technologies, bioaccessibility and applications, Food Res. Int. 132 (2020) 109035, https://doi.org/10.1016/j.foodres.2020.109035.
[103] J.C. Kuszewski, P.R.C. Howe, R.H.X. Wong, Evaluation of cognitive performance following fish-oil and curcumin supplementation in middle-aged and older adults with overweight or obesity, J. Nutr. 150 (2020) 3190–3199, https://doi.org/10.1093/jn/nxaa299.
[104] M.S. Uddin, A.L. Mamun, M. Rahman, P. Jeandet, A. Alexiou, T. Behl, S. Sarwar, et al., Natural products for neurodegeneration: regulating neurotrophic signals, Oxid. Med. Cell. Longev. 2021 (2021) 8820406, https://doi.org/10.1155/2021/8820406.
[105] S. Bawari, D. Tewari, S. Argüelles, A.N. Sah, S.F. Nabavi, S. Xu, et al., Targeting BDNF signaling by natural products: novel synaptic repair therapeutics for neurodegeneration and behavior disorders, Pharmacol. Res. 148 (2019) 104458, https://doi.org/10.1016/j.phrs.2019.104458.
[106] B. Yang, G. Luo, C. Zhang, L. Feng, X. Luo, L. Gan, Curcumin protects rat hippocampal neurons against pseudorabies virus by regulating the BDNF/TrkB pathway, Sci. Rep. 10 (1) (2020) 22204, https://doi.org/10.1038/s41598-020-78903-0.
[107] R. Wang, Y.H. Li, Y. Xu, Y.B. Li, H.L. Wu, H. Guo, J.Z. Zhang, et al., Curcumin produces neuroprotective effects via activating brain-derived neurotrophic factor/TrkB-dependent MAPK and PI3K cascades in rodent cortical neurons, Prog. Neuro-Psychopharmacol. Biol. Psychiatry 34 (2010) 147–153, https://doi.org/10.1016/j.pnpbp.2009.10.016.
[108] N. Kandezi, M. Mohammadi, M. Ghaffari, M. Gholami, M. Motaghinejad, S. Safari, Novel insight to neuroprotective potential of curcumin: a mechanistic review of possible involvement of mitochondrial biogenesis and PI3/Akt/GSK3 or PI3/Akt/CREB/BDNF signaling pathways, Int. J. Mol. Cell. Med. 9 (2020) 1–32, https://doi.org/10.22088/IJMCM.BUMS.9.1.1.
[109] L. Zhang, Y. Fang, Y. Xu, Y. Lian, N. Xie, T. Wu, et al., Curcumin improves amyloid β-peptide (1-42) induced spatial memory deficits through BDNF-ERK signaling pathway, PLoS One 10 (6) (2015), e0131525, https://doi.org/10.1371/journal.pone.0131525.
[110] R. Wang, Y.B. Li, Y.H. Li, Y. Xu, et al., Curcumin protects against glutamate excitotoxicity in rat cerebral cortical neurons by increasing brain-derived neurotrophic factor level and activating TrkB, Brain Res 1210 (2008) 84–91, https://doi.org/10.1016/j.brainres.2008.01.104.
[111] A. Shakeri, M.R. Zirak, A.W. Hayes, R. Reiter, G. Karimi, Curcumin and its analogues protect from endoplasmic reticulum stress: mechanisms and pathways, Pharmacol. Res. 146 (2019) 104335, https://doi.org/10.1016/j.phrs.2019.104335.
[112] G. Chen, Z. Fan, X. Wang, C. Ma, K.A. Bower, X. Shi, et al., Brain-derived neurotrophic factor suppresses tunicamycin-induced upregulation of CHOP in neurons, J. Neurosci. Res. 85 (8) (2007) 1674–1684, https://doi.org/10.1002/jnr.21292.
[113] K. Shimoke, T. Utsumi, S. Kiri, M. Nishimura, H. Sasaya, M. Kudo, T. Ikeuchi, Prevention of endoplasmic reticulum stress-induced cell death by brain-derived neurotrophic factor in cultured cerebral cortical neurons, Brain Res 1028 (2004) 105–111, https://doi.org/10.1016/j.brainres.2004.09.005.